IDENTIFYING EXTRACELLULAR MATRIX PROTEIN DYNAMICS IN SKELETAL MUSCLE HYPERTROPHY FOR REGENERATIVE THERAPIES

by

Alita Miller

A Thesis

Submitted to the Faculty of Purdue University

In Partial Fulfillment of the Requirements for the degree of

Master of Science in Biomedical Engineering

Weldon School of Biomedical Engineering

West Lafayette, Indiana

May 2020

THE PURDUE UNIVERSITY GRADUATE SCHOOL
STATEMENT OF COMMITTEE APPROVAL

Dr. Sarah Calve, Chair
Weldon School of Biomedical Engineering
University of Colorado – Boulder

Dr. Tamara Kinzer-Ursem
Weldon School of Biomedical Engineering

Dr. Craig Goergen
Weldon School of Biomedical Engineering

Approved by:
Dr. George R. Wodicka

Dedicated to my family and friends.

ACKNOWLEDGMENTS

I would like to acknowledge Dr. Sarah Calve for her guidance and support through my research studies in the Musculoskeletal Extracellular Matrix Laboratory. Special thank you to Kathryn Jacobson for providing insight on mass spectrometry data analysis.

I would like to acknowledge my committee members, Dr. Tamara Kinzer-Ursem for her insight regarding bioorthogonal labeling and click chemistry-based experiments and Dr. Craig Goergen for providing of surgical equipment and advice for mouse surgery protocols.

I would like to acknowledge Dr. Uma Arval and the Purdue Proteomic Facility for their assistance on proteomic experiments.

This project was funded by National Institutes of Health: R01 AR071359 and DP2 AT009833.

TABLE OF CONTENTS

LIST OF ABBREVIATIONS

1XL	1X Laemmli buffer
ACN	Acetonitrile
Aha	L-azidohomoalanine
BONCAT	Bioorthogonal non-canonical amino acid tagging
ChABC	Chondroitinase ABC
ECM	Extracellular matrix
HAase	Hyaluronidase
HPLC	High performance liquid chromatography
THPTA	Tris-hydroxypropyltriazolylmethylamine
LC-MS/MS	Liquid chromatography-tandem mass spectrometry
LFQ	Label free quantification
M	Plantaris muscle without aponeurosis
Met	Methionine
NSP	Newly synthesized protein
P	Plantaris muscle with aponeurosis
SDS-PAGE	Sodium dodecyl sulfate polyacrylamide gel electrophoresis
SLRPs	Small leucin-rich proteoglycans
T	Plantaris tendon
TBS	Tris buffered saline
TBST	Tris buffered saline + 0.05% Tween 20
TFA	Trifluoroacetic acid
VML	Volumetric muscle loss

LIST OF TABLES

LIST OF FIGURES

ABSTRACT

Skeletal muscle regeneration is hindered in severe injuries and degenerative diseases, including volumetric muscle loss (VML), due to the failure of current treatments to induce functional tissue growth. Various biological functions in skeletal muscle are supported by the extracellular matrix (ECM), a collection of proteins and glycosaminoglycans. *In vivo* studies on murine plantaris muscle hypertrophy indicate that ECM remodeling facilitates muscle growth, but a global analysis of ECM protein dynamics during skeletal muscle hypertrophy and repair are unknown. Understanding this influence of the ECM can establish instructive cues for regenerative therapies. Here, we define global proteomic changes throughout stages of plantaris muscle hypertrophy, with an emphasis on characterizing ECM proteins. Synergistic ablation of the gastrocnemius and soleus muscles induced a compensatory hypertrophic effect causing a 40% mass increase in the plantaris muscle 28 days post injury. Liquid chromatography-tandem mass spectrometry revealed the differential abundance of 1233 proteins, including 99 ECM proteins, across five time points. After two days of injury, a significant increase of ECM glycoproteins was observed although the overall collagen abundance decreased. Throughout the duration of injury, the relative abundance of type I collagen decreased while there was an increase of proteins associated with type I collagen fibrillogenesis (types III and V) and basement membrane (types IV and VI). Collectively, these results provide a better understanding of ECM dynamics throughout skeletal muscle hypertrophy. Future studies will evaluate protein synthesis by using non-canonical amino acids to identify newly synthesized proteins. Temporal analysis of protein dynamics symbolic to injury and tissue growth will provide tissue engineers with precise information to develop successful regenerative therapies to restore functional muscle in VML.

Keywords: skeletal muscle, compensatory hypertrophy, extracellular matrix, mass spectrometry

CHAPTER 1. INTRODUCTION

Voluntary motor function of the body is executed by skeletal muscle and is critical in everyday life. Skeletal muscle and has the natural ability to regenerate and repair; however, these processes are hindered in severe skeletal muscle injuries. One example is volumetric muscle loss (VML), which is a result of trauma that leaves muscles with limited or no functional capabilities. Regeneration of functional muscle tissue has been studied in VML animal models but current research has only been able to show a ~16% beneficial effect in restoring functional capacity [1]. Fibrosis is a large contributor to the loss of functionality in VML and is due to an increased deposition of extracellular matrix (ECM) [2,3]. The ECM is a collection of proteins and glycosaminoglycans that provides mechanical stability and biochemical signaling within damaged tissue to facilitate the reconstruction of functional skeletal muscle [4-6]. However, the delayed removal of damaged tissues following VML promotes inflammation and fibrosis that disrupts natural reconstruction [3]. Current treatments that utilize the role of the ECM during repair via engineered scaffolds have limited clinical value due to the lack of knowledge of environmental cues including source matrix and signaling molecules [7]. In order to study ECM protein dynamics throughout repair, a mode of tissue remodeling is required. Skeletal muscle hypertrophy is a common form of tissue repair and regeneration used for identifying molecular mechanisms that regulate increased muscle strength [8]. Here, we evaluate the compensatory hypertrophy of the plantaris muscle to understand the dynamics of ECM proteins during skeletal muscle growth and repair. This study will enhance regenerative therapies to restore function in VML by providing an *in vivo* analysis of source matrix and crucial molecular signals during skeletal muscle tissue growth.

Compensatory hypertrophy is induced in the plantaris muscle of the murine hindlimb via synergistic ablation of the gastrocnemius and soleus muscles (Figure 1.1). Briefly, an overload of forces is translated to the plantaris muscle and causes a hypertrophic effect. This injury model was first described by Dr. A. L. Goldberg and has been used to study many hypertrophic responses [9]. The following time points of injury have been characterized based on the current understanding of plantaris muscle overload [10-12]: uninjured control baseline (day 0, D0), inflammatory response (D0.5 – D5), onset of hypertrophy (D5 – D10), and restoration of homeostasis (D14 – D28).

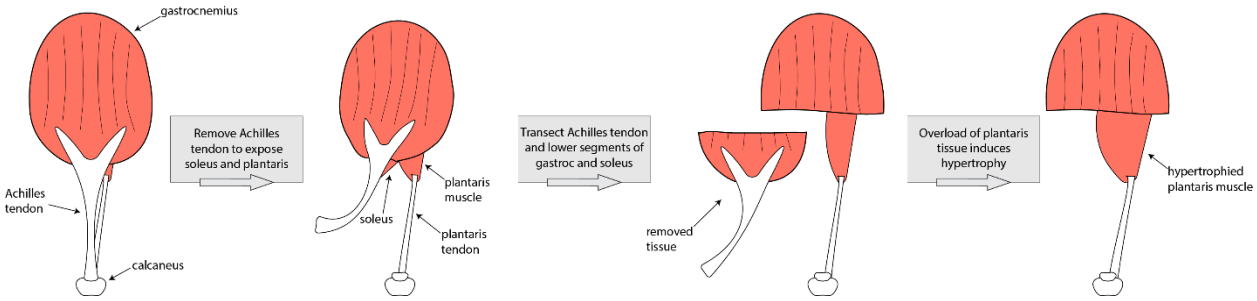

Figure 1.1: Synergistic ablation procedure. Removal of the gastrocnemius and soleus synergist muscles in the hindlimb induce overload of the plantaris muscle which results in hypertrophy. Figure designed in Adobe Illustrator 2019.

Many studies of induced skeletal muscle hypertrophy have focused on identifying the role of satellite cells [13], cell-ECM interactions [14] and muscle specific miRNA expression [15] throughout different stages of tissue remodeling. When focusing on the molecular mechanisms in hypertrophy, increased mechanical loading drives a positive net protein synthesis where the rate of synthesis outweighs protein degradation [16]. Regarding the ECM, this hypertrophy model has only been used to study a handful of proteins to understand the distribution of the ECM during injury and repair [17,18].

Liquid chromatography-tandem mass spectrometry (LC-MS/MS) provides a unique global protein analysis as opposed to individual protein characterization methods such as western blotting, enzyme-linked immunosorbent assays, immunohistochemistry staining, or analysis of gene expression. It has been extensively used to analyze the proteomic composition of various skeletal muscle tissues including many biological models of insulin deficiency [19-21] and recently have evaluated the proteome after injury [22-24]. Of the studies that identified a global protein analysis in injured muscle, only one study focused on skeletal muscle hypertrophy using a follistatin-induced hypertrophy model [24]. Follistatin alters biological processes and protein synthesis while the overload hypertrophy model used in this study resembles the natural process of increased mechanical loading to promote hypertrophy. Overall, LC-MS/MS has shown great promise for skeletal muscle analysis while only two studies have used this technique to focus on ECM proteins, termed the matrisome [25,26]. A global proteomic analysis of ECM proteins during muscle growth and development remains unknown and was observed in this study by quantifying relative protein intensities throughout overload.

In addition to protein quantifications, we describe a method to identify newly synthesized proteins (NSPs) during skeletal muscle hypertrophy to give greater insight on explicit temporal dynamics. Labeling of NSPs using bioorthogonal non-canonical amino acid tagging (BONCAT) has enhanced the identification of potentially critical proteins during various biological processes [27]. Briefly, L-azidohomoalanine (Aha), a non-canonical methionine (Met) analog, incorporates into NSPs which are then tagged with an alkyne-biomolecule via copper-assisted click chemistry (Figure 1.2) [28,29]. Our lab has previously demonstrated BONCAT can identify NSPs in murine tissue [30].

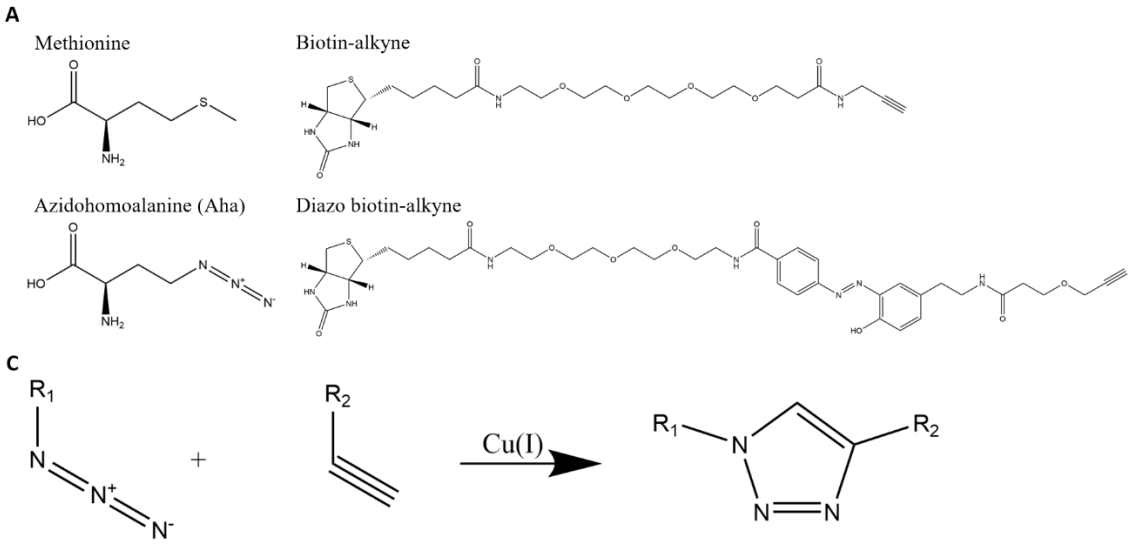

Figure 1.2: Molecular mechanism for the cycloaddition of azide and alkyne. (A) Methionine (top) and the Aha (bottom) analog molecular structures. **(B)** Biotin-alkyne (top) and diazo biotin-alkyne (bottom) molecular structures. **(C)** Copper(I) catalyzed azide-alkyne cycloaddition following [29]. Molecular structures were designed using ChemDraw.

In this study, plantaris muscle hypertrophy was induced by synergistic ablation and corresponding changes in matrisome dynamics were quantified by LC-MS/MS. We evaluate the response after 0, 2, 7, 14, and 28 days of overload to distinguish the adaptation of ECM proteins throughout the extensive process of skeletal muscle injury and repair. Major ECM proteins, including collagens, glycoproteins, and proteoglycans, were differentially expressed at the various stages of overload. The overall relative abundance of collagen decreased immediately after injury while the abundance of glycoproteins significantly increased. Specific protein trends were identified for biological processes and molecular functions including collagen fibrillogenesis, basement membrane

stability, and prevention of fibrosis. The feasibility of labelling NSPs in injured plantaris muscles was established via western blot analysis. Future work will use both BONCAT and LC-MS/MS to map the temporal distribution of ECM protein synthesis, as an addition to the current understanding of protein abundance, during plantaris muscle hypertrophy. Ultimately, these results will provide tissue engineers with instructive cues to develop successful regenerative therapies that restore functional tissue in injuries of VML.

CHAPTER 2. METHODS AND MATERIALS

Reagents for LC-MS/MS were high performance liquid chromatography (HPLC)-grade and purchased from Sigma-Aldrich (St. Louis, MO) unless otherwise noted. Reagents for gel electrophoresis were purchased from Bio-Rad unless otherwise noted. Quantitative data was analyzed with Microsoft Excel 2016 (for data handling) and GraphPad Prism 8 (for data visualization and statistical analysis).

2.1 Animal Models

Male C57BL/6 wild-type mice aged 8 – 10 weeks were purchased from The Jackson Laboratory. Animals were allowed a minimum of three days to adapt to the holding facility maintained on a 12/12-hour light/dark rotation. Surgeries were completed under the conditions of the Purdue Animal Care and Use Committee (PACUC) protocol #1908001934. PACUC adheres to regulations of the USDA and the United Stated Public Health Service in accordance with the Animal Welfare and Purdue's Animal Welfare Assurance to ensure animal safety.

2.2 Synergist Ablation

Synergistic ablation of the gastrocnemius and soleus muscles was conducted to induce overload on the plantaris muscle. Prior to surgery, surgical tools were autoclaved for 30 minutes at 121˚C. Sterile gauze drapes and a glass bead sterilizer were used during and between surgeries to maintain aseptic technique. Isoflurane inhalation of 3 – 5% was used to anesthetize mice with weight-dependent volumetric flow rates controlled using the SomnoSuite Low-Flow Anesthesia System. Anesthesia was maintained at a level of 1 – 2% isoflurane during the length of the procedure. Ophthalmic solution was applied before starting surgical preparation to prevent cornea drying. Fur was removed from the surgical area with depilatory cream (Veet 3-in-1 Gel Cream) followed by three scrubbing rotations of povidone iodine (PDI®) and warmed saline.

After sterile preparation, a 3mm incision was made on the posterior hindlimb. The Achilles tendon was separated from the plantaris tendon by sliding Dumont #5 fine tip forceps (Fine Science Tools: #91150-20) between the two. The Achilles tendon was transected at the distal end with Vannas

spring scissors (Fine Science Tools: #91500-09). Care was taken to remove a 1mm segment of the Achilles tendon along with the lower third of the gastrocnemius and soleus muscles. Halsted-Mosquito Hemostat suture forceps (Fine Science Tools: 91308-12) were used to close the incision via the interrupted stitching technique with polypropylene 6-0 blue monofilament PC-1 sutures (Surgical Specialties: #J8617N). The first hindlimb was completed and closed before proceeding to the contralateral limb. Mice were allowed to recover from anesthesia for at least 5 minutes before being returned to a new cage for single housing. All surgeries were complete between the hours of 10:00 AM and 1:00 PM. Mice received three doses of 1.5μg buprenorphine 8 – 12 hours apart, starting immediately after closure of the incision. The analgesic injections were given under anesthesia to remove the possibility of suture reopening while scruffing. Mice were monitored for 7 days post-surgery for changes in eating, drinking, or disturbances in ambulation.

2.3 Aha-labeling of Newly Synthesized Proteins (NSPs)

L-azidohomoalanine (Aha, Figure 1.2A, Click Chemistry Tools) was solubilized in PBS and adjusted to pH 7.4, using NaOH, at a stock concentration of 10mg/mL. Aliquots were sterilized by syringe filtration and stored at -20˚C until use. Subcutaneous injections were used to administer 0.1mg Aha per g mouse, 6 hours prior to tissue collection. Vehicle control mice were injected with similar weight-dependent volumes of sterile PBS. The scruffing technique was used to stabilize mice during injection. Peak labeling was assumed to be 6 hours based on previous incorporation studies [31]. Animals were injected in the early morning (6:00 – 9:00 AM) of the last day of overload in order to be harvested midday (12:00 – 3:00 PM).

2.4 Plantaris Muscle Collection

Experimental mice were subject to compensatory hypertrophy for 2, 7, 14, or 28 days (n=7, 7, 3, and 4 respectively) while non-injured mice (n=9) were used as a control baseline. Euthanization was carried out by CO_2 inhalation followed by cervical dislocation and mice were weighed prior to tissue harvest. Images were taken throughout the dissection with a Leica DFC450 microscope to visualize anatomical changes. After the skin was removed, hindlimbs were severed from the mouse with muscle groups still intact. Lungs were collected as an internal control to confirm Aha-labeling. All tissues were kept in ice cold PBS during the duration of the harvest. The remnants of

the gastrocnemius and soleus muscles were separated from the plantaris muscle by gently pulling off or cutting connective tissue when necessary. Plantaris muscles from both hindlimbs were removed and separated from the plantaris tendon (T) before being weighed. Full plantaris tissues (P, aponeurosis still intact) were embedded for cryostat slicing while contralateral limbs were further dissected into the muscle (M) and aponeurosis portions before being snap frozen in liquid nitrogen for long-term storage at -80˚C (Figure 2.1).

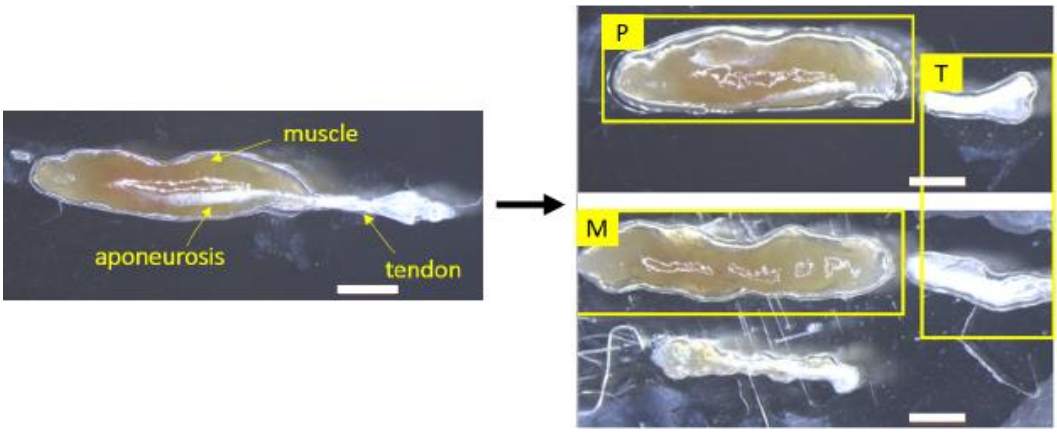

Figure 2.1: Microdissection of P, M, and T tissues. Plantaris tissue is comprised of muscle, aponeurosis, and tendon sections (left) and dissected into the following samples: muscle with aponeurosis (P), muscle without aponeurosis (M), plantaris tendon (T) (right). Scale bars=2mm.

2.5 Overload Quantification

Tissues were blotted dry on a Kimwipe to remove excess PBS. Care was taken to not let the samples dry out during the weighing process. The scale was tared before each sample and allowed to stabilize before noting mass. Positive mass remaining after removing the tissue was subtracted from the original tissue weight. If the scale showed a negative value after tissue removal, the sample was weighed again. Tissue weights were normalized to the overall body weight of the mouse in a mass ratio (mg/g), shown below.

$$Mass\ Ratio\ (MR) = \frac{tissue\ weight\ (mg)}{body\ weight\ (g)}$$

A baseline mass ratio was determined from the average of all non-injured mice (10 – 13 weeks). The mean, standard deviation, and range of data were analyzed to ensure the mass ratios of non-

injured mice did not show large variance. The percent increase from the baseline was determined from individual overload mass ratios of each time point using the equation below.

$$\%\ Increase\ of\ MR = \frac{overload - baseline}{baseline} \times 100\%$$

2.6 Tissue Solubilization

Plantaris tissues were thawed on ice and mechanically disrupted via glass tissue grinders (ACE Glass). Initial solubilization procedures involved grinding tissue in 500µL of 8M urea/100mM ammonium bicarbonate. Briefly, ammonium bicarbonate was solubilized in HPLC-grade water. Only about half of the solvent volume was needed to dissolve urea, directly weighed into conical tube, to a final volume resulting in 8M urea. The solution was vortexed until urea crystals fully solubilized. Overload tissue samples were homogenized in 500µL of PBS pH 7.4/50mM sodium acetate, base buffer for hyaluronidase (HAase) and chondroitinase ABC (ChABC) enzymatic reactions. HAase and ChABC catalyze reactions to cleave hyaluronic acid and sugar chains respectively. Tissue were homogenized on ice until most of the sample was disrupted (tendons did not fully solubilize). Samples were transferred to an Axygen tube using a cut pipette tip to ensure full recovery. Tissues of the same type and labeling (i.e. Aha vs. PBS control) were ground in the same homogenizer after washing with 1mL HPLC-grade water. PBS samples were ground first to ensure no Aha-labeled proteins would get into the sample.

For samples subject to initial enzymatic reactions, HAase was added at a final concentration of 0.5mg/mL and agitated at 37˚C for 6 hours. All agitations were complete in an Eppendorf ThermoMixer F1.5 at 1000rpm. ChABC was added at a final concentration of 0.1U/200µL and agitated at 37˚C for 16 hours. Proteins were precipitated using an acetone technique. Briefly, samples were transferred to 15 mL conical and 4X the volume of cold 100% acetone was added. After overnight incubation at -20˚C, samples were sequentially spun down at 4˚C and 14000rpm for 10 minutes each. Supernatants were discarded and the final pellet was dried for 15 minutes. Pelleted proteins were resolubilized in 500µL fresh 8M urea using pipet tip mechanical disruption.

The Branson Sonifier 450 (Branson) was used to further disrupt all 8M urea solubilized tissue. Samples were sonicated on ice with 15 pulses at output control 3 and 50% duty cycle. A 1-minute

cool down period was allowed between each of 4 cycles in order to prevent protein overheating and shearing.

Lungs (L) and gastrocnemius (G) samples from PBS and Aha-injected mice were homogenized in 500µL fresh 8M urea on ice using a TissueRuptor (Qiagen). Tissue rupture probe tips were rinsed in PBS between samples. As before, PBS control samples were homogenized before the Aha-tagged samples. Furthermore, a fresh probe tip was used for different tissue types. When the wet weight of the tissue exceeded 250mg, 8M urea was added to have a total volume 2 times the weight.

After homogenization, insoluble proteins were pelleted by centrifugation at room temperature (RT) for 5 minutes at 14000rpm. The supernatant was collected, and protein concentrations were quantified using the Pierce 660nm Protein Assay (ThermoFisher Scientific). An aliquot was saved before being subject to click reactions to serve as the unenriched protein sample for LC-MS/MS analysis.

2.7 Liquid Chromatography-Tandem Mass Spectrometry (LC-MS/MS)

Samples of protein previously solubilized in 8M urea, 100µg, were prepared for LC-MS/MS analysis. Proteins were reduced with dithiothreitol (10mM final concentration) at 37˚C with constant agitation for 2 hours. Samples were alkylated with iodoacetamide (final concentration 25mM) at room temperature in the dark for 30 minutes. Urea was diluted to a final concentration of 2M to reduce harsh conditions for enzyme incubations. Protein samples for pre-injury proteomics, therefore not previously deglycosylated, were incubated with ChABC (0.1U/200µL) at 37˚C with constant agitation for 2 hours. Proteins were digested into peptides using three enzymatic steps: (1) LysC (1µg/200µL) for 2 hours, (2) trypsin (3µg/200µL) overnight, and (3) trypsin (1µg/200µL) for 2 hours. Digestion was stopped by acidifying the solution with 0.1% trifluoroacetic acid (TFA).

Peptides were cleaned and concentrated using C18 Silica MicroSpin Columns (The Nest Group). Briefly, columns were conditioned with 100µL 100% acetonitrile (ACN, ThermoFisher Scientific), then equilibrated with 200µL 0.1% TFA in water. Centrifugation steps were completed at room temperature and 1000rpm for 1 minute or until liquid was cleared from column. Samples were

then added to the columns and washed with an additional 2×200µL 0.1% TFA solution. Peptides were eluted in 100µL 80% ACN + 25mM formic acid and vacuum dried (CentriVap) at 45˚C for 400 minutes. Dried peptides were resuspended in 3% ACN + 0.1% formic acid and peptide concentrations were normalized to 0.5µg/µg using the Pierce Quantitative Colorimetric Peptide Assay (ThermoScientific).

2.8 Proteomic Analysis

Raw files were analyzed by MaxQuant (versions 1.6.1.0 and 1.6.7.0) [32]. Peptide sequences were searched against the *Mus musculus* FASTA file (canonical and isoform, 12/2019). The following post-translational modifications were used: oxidation of methionine, deamidation of asparagine, hydroxylation of proline and lysine, methionine replacement by Aha (only when using Aha-labeled samples). Match between runs was enabled between biological replicates. Specific parameters for the two datasets analyzed (pre-injury and overload proteomics) are reported in Appendix A.

The MaxQuant output file 'proteinGroups.txt' was used to analyze protein intensities. A group of proteins were filtered out of subsequent data analysis for the following reasons: (1) razor and unique peptide count was less than two, (2) the summed protein intensity across all samples was equal to zero, (3) the protein was marked as a reverse hit or contaminant, (4) neither protein or gene name was listed, and (5) the protein was only identified within one biological replicate. The following proteins were incorrectly marked as contaminant proteins, but were kept for analysis: TPM2, GSN, CYCS, PFN1, THBS1, SERPINC1, FBLN1, LUM. Proteins were categorized into the following proteomic compartments using a list derived from The Matrisome and Gene Ontology Projects [33,34]: cytosolic, nuclear, membrane, cytoskeletal, matrisome-associated, and core matrisome. Matrisome compartments were further classified into core matrisome (collagens, proteoglycans, and ECM glycoproteins) and matrisome-associated proteins (ECM-Affiliated proteins, ECM regulators, and secreted factors) [33].

Raw intensities were used when proteins were being compared within a sample (*i.e.* percentage of matrisome coverage) while label free quantification (LFQ) intensities were used when comparing proteins across multiple samples (*i.e.* protein significance over time). The following sections detail the specific quantitative analysis completed for each LC-MS/MS experiment. Recall, the following

nomenclature was used: plantaris muscle with aponeurosis (P), muscle without aponeurosis (M), and plantaris tendon (T).

2.8.1 Pre-injury Proteomics

LC-MS/MS was completed on 8M urea solubilized P, M, and T samples (n=3). Insoluble pellets of M and T were also analyzed (n=3 and 2 respectively). Table A.1 details the MaxQuant parameters. Briefly, soluble and insoluble samples were separated into two parameters groups and LFQ normalization was employed across each group, separately.

The total number of proteins identified across all samples were counted and delineated into the respective cellular compartment. Raw intensities were used to identify cellular compartment percentages for each tissue type, soluble and insoluble. Matrisome percentages were further analyzed by one-way ANOVA to determine the significance across either tissue type or solubility. Pre-injury proteomics also was used to identify what proteins may not be soluble for Aha enrichment. Proteins that were exclusively found in either P or M insoluble tissue samples were listed and ranked in order of greatest abundance.

Individual matrisome proteins were analyzed between P and M soluble samples to identify the significance of the aponeurosis. LFQ normalization is typically used when comparing proteins across a sample, but the accuracy decreases when normalizing across different tissue types. Here, LFQ normalization was employed across soluble P, M, and T, which could result in false analysis of ECM protein within just P and M. Therefore, both raw intensity normalization and LFQ intensities were used to evaluate the aponeurosis significance. Individual protein raw intensities were normalized so that the total sum of raw intensities within a sample was the same across all soluble P and M replicates. Intensities were $\log_2$ transformed before being analyzed by a two-sample and two-tailed t-test. Averages of the P and M samples were subtracted to find the fold change. Volcano plots were created for both normalization techniques showing overall proteome and matrisome specific values.

2.8.2 Overload Proteomics

LC-MS/MS was completed on unenriched Aha-labeled M samples from 0, 2, 7, 14, and 28 days of overload (n=3). PBS-labeled non-injured tissue was also analyzed. Tissue solubilization included HAase and ChABC incubations before 8M urea extraction. Table A.2 details the MaxQuant parameters. Briefly, methionine to Aha replacement was included as a variable modification and LFQ normalization was employed across all samples.

The total number of proteins identified across all samples were counted and delineated into the respective cellular compartment. In addition, matrisome proteins were counted and delineated into the respective ECM classifications. For analysis across time points, the 0-day PBS sample was dropped to remove potential variability. Raw intensities were used to identify cellular compartment percentages and ECM classifications for each time point. Cellular compartment percentages were further analyzed by two-way ANOVA to determine the significance across time and cellular compartment, with an emphasis on cytoskeletal and matrisome percentages. ECM classifications were analyzed by two-way ANOVA with time and classification as the two factors.

To look at the temporal dynamics of individual proteins, a row z-score was calculated. A center intensity for each protein was calculated by averaging the LFQ intensities across all replicates. A row z-score was calculated for each matrisome protein using the equation below. Matrisome proteins were also subject to one-way ANOVA using LFQ intensities to identify the significance of different time points of overload.

$$Z - score = \frac{LFQ_{replicate} - average\ of\ protein\ LFQ}{standard\ deviation\ of\ protein\ LFQ}$$

Lastly, a comparison between PBS and Aha tissues was evaluated to ensure unenriched samples have a similar starting composition. Raw intensities were used to find the average percentages of proteins identified in both injection types. PBS percentages were plotted against Aha percentages for each to visualize the relation to a trendline with the slope of 1.

2.9 Cell Culture

C2C12 mouse myoblasts (ATCC, CRL-1772) were used for control purposes when confirming Aha-labeling. Cells were cultured in methionine-free Dulbecco's Modified Eagle's Medium (Gibco) supplemented with cysteine, 1X penicillin/streptomycin, 1% glutagro supplement (Corning), and 10% fetal bovine serum (Atlanta Biologicals). L-azidohomoalanine (Aha, Click Chemistry Tools) or methionine was added to media at 10mg/mL for 24 hours. Cells were dissociated from culture dishes using Trypsin-EDTA then pelleted by 5-minute centrifugation at 200×g and stored at -20˚C until further use. C2C12 cells were lysed in 500µL fresh 8M urea by mechanical disruption with a pipette tip before use.

2.10 Cycloaddition Click Reaction

Click reactions were performed to analyze Aha-labeled proteins. Samples were clicked in a total volume of 400µL using freshly prepared reagents solubilized in MilliQ water unless otherwise stated. Table 2.1 details the ratios of stock reagent volumes to the total click reaction volume and the exact volumes for an 400µL reaction.

Table 2.1: Experimental details for azide-alkyne click reactions.

Stock Solution	**Ratio (v/v)**	**Volume Added**	**Final Concentration**
Total sample	29:50	232µL	2mg protein
0.5M iodoacetamide (VWR)	1:20	20µL	25mM
10mM biotin-alkyne OR diazo biotin-alkyne (Figure 1.2A, Click Chemistry Tools)	1:200	2µL	0.05mM
100mM tris-hydroxypropyltriazolylmethylamine (THPTA, Click Chemistry Tools)	1:10	40µL*	10mM
50mM cupric sulfate, 5-hydrate ($CuSO_4$, Macron Chemicals)	1:25	16µL*	2mM
100mM aminoguanidine hydrochloride, pH 7.4 (Sigma-Aldrich)	1:5	80µL	0.002mM
400mM (+)-sodium L-ascorbate (Sigma-Aldrich)	1:40	10µL	10mM

*A mixture of THPTA and $CuSO_4$ was added simultaneously at a total volume of 56µL

A total of 2mg total protein was clicked and diluted to 232µL using 8M urea. Samples were alkylated by iodoacetamide at room temperature for 30 minutes while rotating end-over-end in the dark. The remaining reagents were added in the following order: (1) biotin-alkyne or diazo-biotin

alkyne, (2) THPTA and $CuSO_4$ mixture, (3) aminoguanidine, and (4) sodium ascorbate. Biotin-alkyne was added for samples that were analyzed via western blot and diazo biotin-alkyne was used for samples processed for LC-MS/MS analysis. Reactions were rotated end-over-end for 2 hours at room temperature. Acetone precipitation was used to remove unreacted click reagents from the proteins.

2.11 SDS-PAGE

Proteins were solubilized in a 1X Laemmli buffer (1XL) + 5% 2-mercaptoethanol (ThermoFisher Scientific) and boiled with constant agitation at 95˚C for 5 minutes unless otherwise noted. The Pierce 660nm Protein Assay was used to identify protein concentrations. For every sample, 30µg of protein was added to each lane of Mini-PROTEAN TGX Stain-Free Gels unless otherwise noted. Precision Plus Protein Dual Color Standards ladder was diluted 1:100 in 1XL and added for protein molecular weight reference. Fine tip gel loading tips (VWR) were used to ensure precise loading. Gels were run on a Bio-Rad PowerPac HC at 170V for 42 minutes. Gels were either stained with GelCode Blue Safe Protein Stain (ThermoFisher Scientific) or transferred for western blot analysis. Stained gels were rocked at room temperature for at least 2 hours followed by overnight removal of excess dye with water before being imaged.

2.12 Western Blot

After SDS-PAGE, gels were placed in the Trans-Blot Turbo Transfer Pack and transferred to a 0.2µm polyvinylidene fluoride membrane using the Trans-Blot Turbo Transfer System. Air bubbles were rolled out of the stack after each layer was added to limit interference with protein transfer. The following transfer parameters were used: 25V maximum, constant 1.5A, and 5 minutes. After transfer, membranes were blocked in Pierce Protein-Free (TBS) Blocking Buffer (ThermoScientific) for 1 hour at RT. Protein band autofluorescence was captured before initiating antibody staining. All images were taken using the Azure c600 imaging system (Azure Biosystems) and cSeries Capture Software. Each channel was exposed for three seconds for every gel and membrane that was imaged.

Streptavidin 680RD IRDye (LI-COR, 1:5000) was used to probe biotinylated proteins. This was diluted in a 1:1 solution of blocking buffer:tris buffered saline + 0.05% Tween 20 (TBST). Membranes were incubated with the streptavidin antibody overnight at 4˚C with gentle rocking, followed by washing with TBST 3× and TBS 2×5 minutes each. Membranes were then imaged as described above.

2.13 Statistical Analyses

One-way ANOVA followed by Tukey's post-hoc analysis was used to determine the significance of matrisome percentage over time. Two-way ANOVA followed by Tukey's post-hoc analysis was used to identify the significance of ECM classification and time.

Two-tailed t-tests were used to determine the significance of the aponeurosis on individual protein intensities. Both normalized raw intensities and LFQ intensities were $\log_2$ transformed to ensure the data resembled a Gaussian distribution. All intensities were transformed in order to compare numerical (p-value<0.05) and biological significance ($\log_2$(fold change) > ± 1) results across different proteins on volcano plots.

One-way ANOVA tests were used to determine the significance of overload on individual protein intensities. LFQ intensities were tested for normality (Shapiro-Wilk test) and equal variance (Brown-Forsythe test) within each protein. If the assumption tests failed, the data was $\log_2$ transformed and the assumptions were tested again. Significance testing was completed on original LFQ intensity values if the assumptions were met or transformed intensities failed assumption tests.

CHAPTER 3. RESULTS

3.1 Overload Model

Calcaneus scabbing and blood content variations were observed during overload. Synergistic ablation of the gastrocnemius and soleus muscles was used to overload plantaris muscles for 0, 2, 7, 14, or 28 days. Images of the posterior hindlimb directly after cervical dislocation revealed scabbing of the skin surrounding the calcaneus bone (Figure 3.1A), blood vessel reconstruction on the medial hindlimb (Figure 3.1B), and increased blood content in the plantaris muscle (Figure 3.1C).

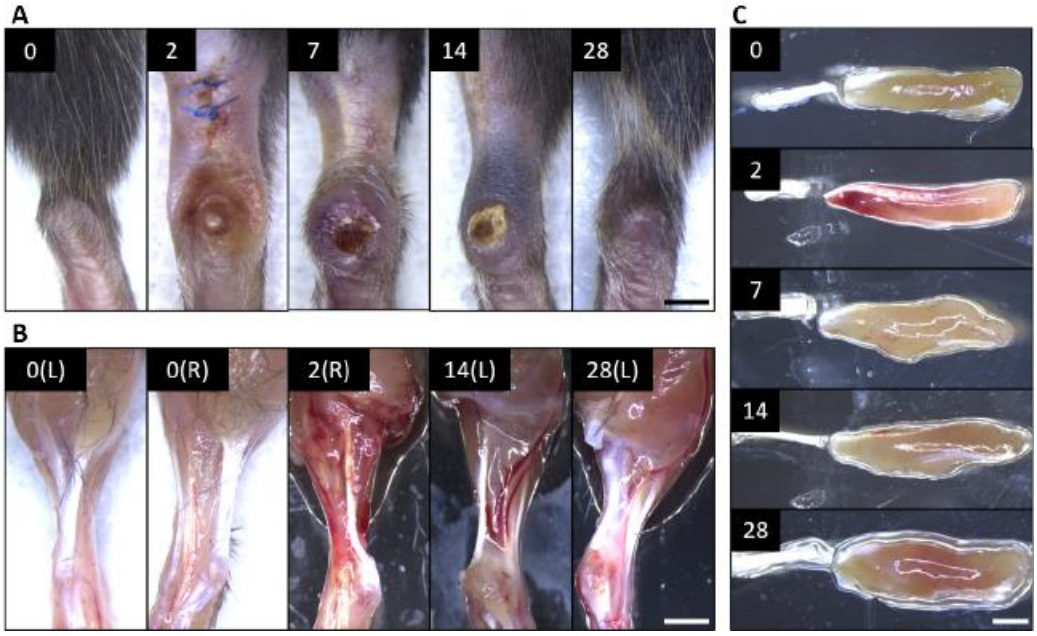

Figure 3.1: Anatomical changes after 0, 2, 7, 14, and 28 days of compensatory hypertrophy. (A) External hindlimb images show calcaneus skin scabbing commenced after 2 days then healed after 28 days. **(B)** Internal hindlimb images show blood vessel reconstruction on the medial side of the left (L) or right (R) hindlimb mostly at 14 days. **(C)** Plantaris muscles had increased blood content at 2 days but decreased over time. Scale bars=2mm.

No infection was seen and there were no observed differences in mouse ambulation before and after surgery. Sutures had fallen or been chewed out after three days which did not limit the skin healing process. The observed scabbing was thought to have been due to the increase of force on a smaller and more localized area after removal of the Achilles tendon. Typically, only one

hindlimb per mouse had calcaneus scabbing, but the tissue weights within the scabbed hindlimb did not differ from the weights of the scab-free limb. Scab size was reduced over time as the skin fully healed and fur grew back by 28 days. After removing the skin, blood vessel reconstruction was observed on the medial side of the hindlimb. This adaptation was seen after 14 days of overload as the 2 days timepoint was dominated by inflammation and vessels were not as prominent after 7 days. Newly formed vessels indicate a greater abundance of nutrients provided to the plantaris, which is located on the medial side of the hindlimb. After removing external muscles, the plantaris itself revealed an increase in blood content during earlier timepoints. Internal blood remained visible at 28 days, where a red tint was visible within the muscle, opposed to the non-visible blood supply within non-injured tissue.

Synergistic ablation of gastrocnemius and soleus muscles showed an increase in plantaris tissue mass. Weights of plantaris muscles were normalized to the overall body weight of the mouse to create a mass ratio (mg/g). Non-injured mice had a mass ratio of 1.05 ± 0.18mg/g and was used as a baseline control. Overloaded plantaris muscles had ratios of 1.12 ± 0.06, 1.24 ± 0.16, 1.17 ± 0.77, and 1.52 ± 0.22mg/g for 2, 7, 14, and 28 days respectively (Figure 3.2A). There was a significant increase in mass ratio after 7 and 28 days of overload from the non-injured control. Plantaris tissue mass ratio showed over a 40% increase from the baseline control mass ratio after 28 days of overload (Figure 3.2B).

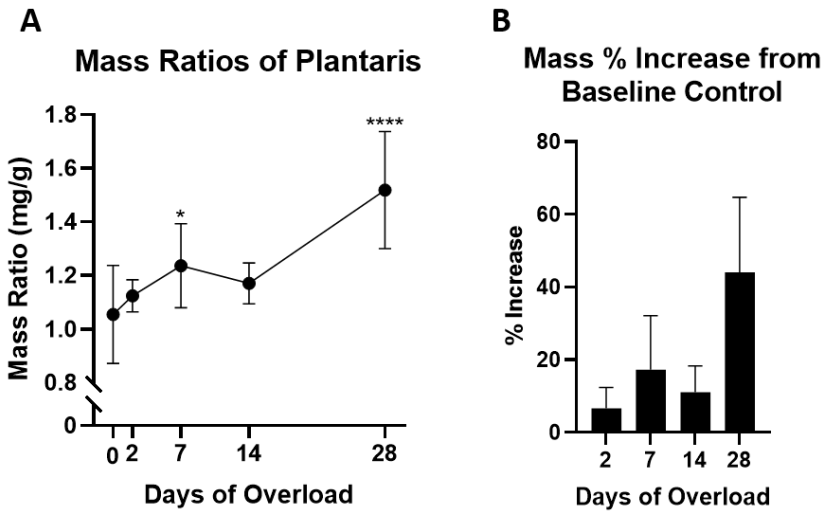

Figure 3.2: Mass ratios of plantaris tissue during overload. Tissues weights were normalized to the overall body weight of the mouse **(A)** Mass ratio of P samples subject to compensatory hypertrophy for 0, 2, 7, 14, and 28 days (n=9, 7, 7, 3, and 4 respectively). **(B)** Percent increase of mass ratios from baseline control for similar data in A. Data is represented as a mean ± standard deviation where biological replicates are averaged from left and right hindlimbs. One-way ANOVA post-hoc analysis shows significance of $^{*}p<0.05$ and $^{****}p<0.0001$.

3.2 Pre-injury Proteomic Analysis

Proteins from all compartments were identified. Uninjured tissues were processed to determine if LC-MS/MS was a feasible method to identify ECM proteins within plantaris muscle tissue. Single buffer solubilization requires a stringent buffer to denature the highly cross-linked proteins in muscle tissue but must be compatible with protein identification assays. Here, uninjured plantaris tissues were solubilized in 8M urea and diluted to 2M urea for enzymatic digestion before LC-MS/MS identification. Single buffer solubilization was able to resolve matrisome proteins without the use of a tissue fractionation technique. After filtering out proteins that did not meet analysis criteria, a total of 1316 proteins were identified with 104 of those being core matrisome or matrisome-associated (Table 3.1). Soluble samples contain a majority of the ECM proteins and reveal the proteins amenable for Aha enrichment, a technique which requires protein solubility. Identification of insoluble proteins allows us to determine potential NSPs that will not be revealed by Aha enrichment.

Table 3.1: Cellular compartment protein counts for pre-injury proteomics.

Sample / Compartment	All	Soluble			Insoluble	
		P	M	T	M	T
Total	1316	1052	1117	598	1000	353
Cytosolic	419	347	371	142	313	74
Nuclear	296	245	263	115	216	61
Membrane	268	205	216	121	226	60
Cytoskeletal	229	190	206	125	186	81
Matrisome (Core, Associated)	104 (66, 38)	65 (38, 27)	61 (37, 24)	95 (61, 34)	59 (39, 20)	77 (53, 24)

Matrisome percentages for P and M were significantly less than that of T while there was no significance between soluble and insoluble tissue. The percentage of each cellular compartment, based on raw intensities, varied by tissue type and solubility. T had the greatest matrisome percentage, as expected (Figure 3.3A). Both P and M samples had much lower percentages of matrisome, but a higher abundance of cytoskeletal proteins. Matrisome percentage was greater in soluble tissue P when compared to M, but there was no significant difference (Figure 3.3B). These results suggest that the aponeurosis does not have a significant effect when comparing overall matrisome compartment percentages while there may be individual protein differences.

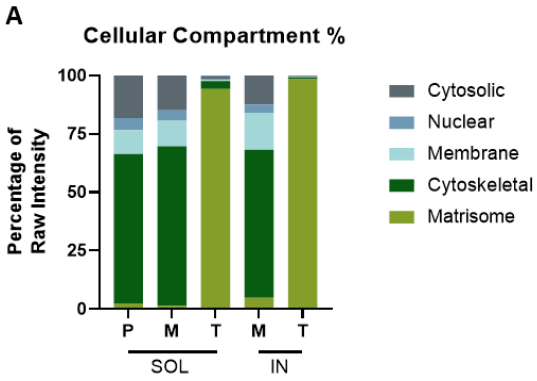

B

		Soluble			Insoluble	
		P	M	T	M	T
Soluble	P	X	ns 0.9066	****	ns 0.3273	****
	M		X	****	ns 0.1013	****
	T			X	****	ns 0.0642
Insoluble	M				X	****
	T					X

Figure 3.3: Cellular compartment analysis of P, M, and T. (A) Cellular compartments percentages for non-injured soluble and insoluble tissue. P = plantaris with aponeurosis, M = plantaris without aponeurosis, and T = plantaris tendon. Data represented as mean for n=3 biological replicates. **(B)** One-way ANOVA post-hoc results for analyzing significance of matrisome percentage across all samples. ****p<0.0001, and ns=not significant (p-value shown>0.05).

For insoluble samples of the same tissue types, the overall cellular compartment spread was similar and matrisome percentages showed no significant difference compared to the soluble sample counterpart (Figure 3.3). Notably, a few proteins were unique to insoluble M or T (Table 3.2).

Type V and type XI collagens were found in soluble tendon but were exclusive to insoluble muscle. These collagens may be of low abundance in soluble muscle tissue and below the LC-MS/MS threshold of identification. On the other hand, elastin was unique in both M and T insoluble samples. Therefore, elastin is not expected to be identified in Aha enrichment studies of NSPs.

Table 3.2: ECM proteins unique to plantaris muscle and tendon insoluble samples.

Muscle (M)		**Tendon (T)**
*COL5A2	**COL5A3	TCHH
LAMA5	TCHH	EMILIN1
ELN	*S100A3	ELN
*COL11A1	*TGFBI	
*MFAP4		

*found in T soluble, **found in T and P soluble

The aponeurosis plays a significant role in plantaris tissue proteomics when looking at specific protein intensities. Although there was no significance between the matrisome coverage of soluble P and M samples, individual protein intensities were significantly different (Figure 3.4). Raw intensities were normalized to a common sum across all replicates within P and M soluble samples. Complete proteome analysis revealed similar amounts of proteins were significant to either P or M samples (Figure 3.4A). Focusing on matrisome proteins, there were more significant proteins found in P than M (Figure 3.4B). COL12A1 is typically associated with tendon tissue and was significantly increased in P samples [35].

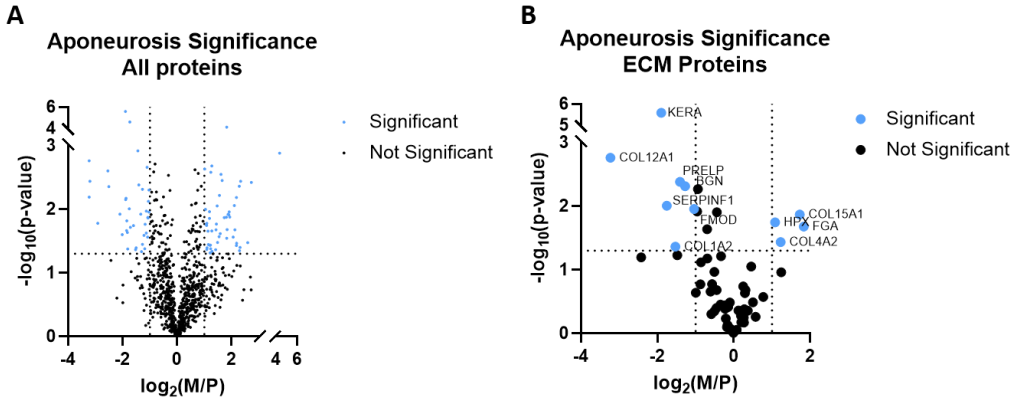

Figure 3.4: Significant effect of the aponeurosis on individual protein identifications using normalized raw intensities. (A) Overall analysis showed a similar number of proteins with a significant increase of relative intensity across P and M samples. **(B)** For ECM proteins, there was a greater number of proteins that showed a significant increase in P samples than M. Significance lines represent p-value < 0.05 and $\log_2$(fold change) > ± 1.

LFQ intensity values were analyzed similarly and showed that normalization technique chosen affects the results (Figure 3.5). Only 665 out of the 1316 total proteins were able to be tested with the t-test due to the lack of intensity values in both samples for a given protein. Intensity values are removed within LFQ normalization when individual protein coverage is extremely different across samples. Tendon samples differ from P and M samples mostly within the cytosolic cellular compartment. The number of proteins that could be statistically analyzed, referred to as t-test valid, was a large decrease from the 1016 t-test valid proteins from raw intensity normalization. Table 3.3 details the number of proteins valid for t-test analysis, significant to P or M, and unique to P or M samples based on normalization technique. Notably, cytosolic proteins lost more LFQ intensities during normalization than any other compartment (338 to 204 t-test valid). Most matrisome proteins that were t-test valid by raw intensity normalization (58/104) were also t-test valid in LFQ normalization (47/104). In each case, there were more significant proteins in the core matrisome of P samples than that of M samples. Proteins that had intensity values unique to either sample type were also noted.

Table 3.3: Count of proteins t-test valid, significant, and unique based on normalization technique.

	Raw Intensity Normalization			**LFQ Intensity**		
Compartment (total count)	**Significant /valid**	**Increased in P:M**	**Unique to P:M**	**Significant /valid**	**Increased in P:M**	**Unique to P:M**
All proteins (1316)	97/1016	42:55	36:101	19/665	17:2	69:159
Cytosolic (419)	31/338	18:13	9:33	4/204	4:0	32:60
Nuclear (296)	20/236	11:9	9:27	4/147	3:1	12:45
Membrane (268)	21/196	5:16	9:20	0/131	0:0	15:26
Cytoskeletal (229)	14/188	1:13	2:18	2/136	1:1	8:24
Matrisome (104) (Core, Assoc.) (66, 38)	11/58 (9/34, 2/24)	7:3 (6:3, 1:1)	7:3 (4:3, 3:0)	9/47 (8/29, 1/18)	9:0 (8:0, 1:0)	2:4 (1:2, 1:2)

The majority of the significant proteins from the overall proteome LFQ analysis were significantly increased in P, different from raw intensity normalization (Figure 3.5A). Extracting ECM proteins from the overall dataset revealed that, similar to raw intensity normalization, there was a greater amount of proteins significantly increased in the P samples (Figure 3.5B). Only 1 protein lost significance when being analyzed with LFQ intensities as opposed to raw intensity normalization. Additionally, the proteins that were found to be significant in LFQ normalization showed numerical significance in raw intensity normalized testing. As seen in raw intensity normalization, COL12A1 showed the greatest biological significant difference.

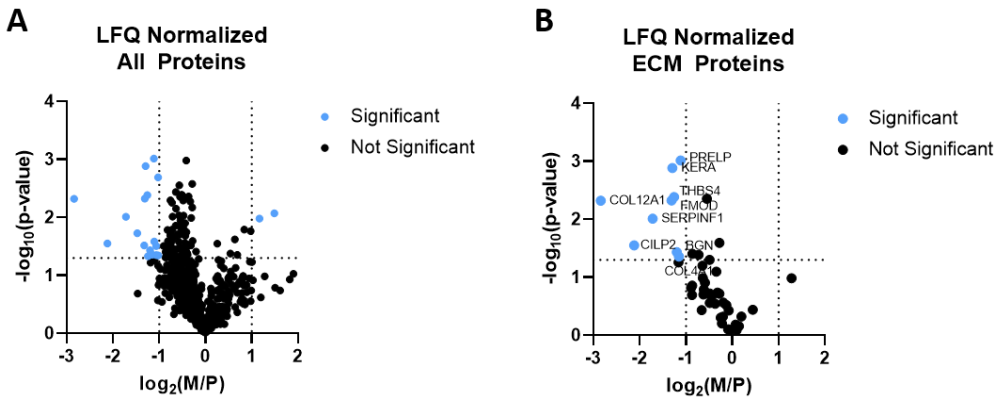

Figure 3.5: Significant effect of the aponeurosis on individual protein identifications using LFQ intensities. (A) Complete proteome analysis showed the majority of proteins have a significant increase of relative intensity in P. **(B)** Matrisome specific analysis shows more significant proteins in P than M. Significance lines represent p-value < 0.05 and $\log_2$(fold change) > ± 1.

These results show that using normalized raw intensities as opposed to LFQ intensities to evaluate the significance of the aponeurosis increases the number of proteins able to be tested without completely altering the results. Overall, the results show that the aponeurosis alters ECM coverage during proteomics and should be dissected from plantaris muscle tissue in LC-MS/MS and other ECM protein analyses.

3.3 Overload Proteomic Analysis

Proteins from all compartments were identified. Synergistic ablation was used to overload plantaris muscles for 0, 2, 7, 14, and 28 days. Plantaris muscles without the aponeurosis were prepared similar to pre-injury proteomic samples but included HAase and ChABC enzymatic reactions in addition. Introducing these incubations before 8M urea solubilization did not alter the number of proteins identified in LC-MS/MS analysis to a large extent. The identified proteins were used for analysis after filtering and removing intensity values identified in a single biological replicate. A total of 1233 proteins were identified with 99 of those being core matrisome or matrisome-associated (Table 3.4). The total protein count for each time point was greater than that of non-injured tissue, suggesting there was an increase of protein synthesis during overload. The greatest number of matrisome proteins were identified during the inflammatory response where a majority of the matrisome-associated proteins (43/45) were identified.

Table 3.4: Cellular compartment protein counts for overload proteomics.

Sample / Compartment	All	0 PBS	0 Aha	2 Aha	7 Aha	14 Aha	28 Aha
Total	1233	792	897	1094	1095	1091	946
Cytosolic	400	245	296	348	351	351	301
Nuclear	273	173	195	249	244	241	193
Membrane	230	173	184	198	206	212	201
Cytoskeletal	231	149	160	208	217	209	183
Matrisome (Core, Associated)	99 (54, 45)	52 (32, 20)	62 (38, 24)	91 (48, 43)	77 (44, 33)	78 (46, 32)	68 (44, 24)

Matrisome proteins were further delineated into the specific ECM classifications (Table 3.5). Of the core matrisome, most proteins were identified as ECM glycoproteins while ECM regulators were the largest number of matrisome-associated proteins. These results may be influenced by the greater number of proteins characterized as glycoproteins and regulators than any other ECM classification [33]. Interestingly, the number of collagens increased throughout overload and all 15 collagens identified by LC-MS/MS were present at 14 and 28 days. Furthermore, the number of proteoglycans, glycoproteins, regulators, and secreted factors were greatest at 2 days of overload. Collectively, these results suggest that there were proteomic differences in plantaris muscle tissue throughout overload.

Table 3.5: ECM classification protein counts for overload proteomics.

Sample / Classification	All	0 PBS	0 Aha	2 Aha	7 Aha	14 Aha	28 Aha
Core Matrisome							
Collagens	15	12	13	13	13	15	15
Proteoglycans	12	9	10	11	10	9	10
ECM Glycoproteins	27	11	15	24	21	22	19
Matrisome-Associated							
ECM-Affiliated Proteins	12	7	9	11	12	11	10
ECM Regulators	28	12	13	27	18	18	12
Secreted Factors	5	1	2	5	3	3	2

Matrisome percentage does not significantly change over time while ECM classification percentages vary. Raw intensities were used to identify the percent distribution of each cellular compartment. Three biological replicates were used for each time point; however, one replicate at the 14-day time point resembled an outlier. All values within this replicate were removed for

quantifications within this document, while the 14-day time point will be completely re-evaluated before publication of these results. The percentage of each cellular compartment varied throughout overload (Figure 3.6A). Matrisome percentage was greatest in non-injured tissue at 8.38% ± 2.08%, and decreased through 2, 7, and 14 days at 8.21% ± 1.42%, 6.82% ± 0.70%, and 6.22% ± 0.33% respectively. Although none of these trends were significant, the decrease may suggest that proteins in other cellular compartments may play a larger role than the matrisome during hypertrophy. By 28 days, the matrisome had increased from the previous time points to 7.94% ± 2.39% but did not reach the non-injured matrisome percentage value.

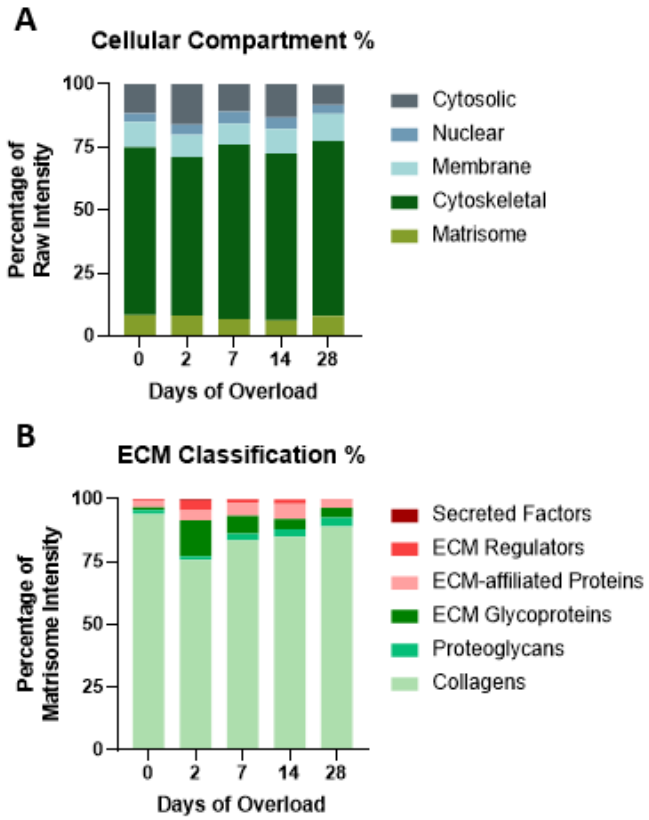

C

	Collagens	Glycoproteins
0 vs. 2	****	****
0 vs. 7	****	**
0 vs. 14	***	ns 0.4935
0 vs. 28	*	ns 0.4007
2 vs. 7	***	***
2 vs. 14	****	****
2 vs. 28	****	****
7 vs. 14	ns 0.9410	ns 0.4355
7 vs. 28	*	ns 0.3041
14 vs. 28	ns 0.2255	ns >0.99999

Figure 3.6: Cellular compartment and ECM classification analysis of overloaded tissue. (A) Cellular compartment and **(B)** ECM classification percentages for overloaded M tissues. Data represented as mean for n=3 biological replicates for all time points (n=2 for 14 days). **(C)** Two-way ANOVA of ECM classification percentages during overload. Tukey's post-hoc analysis results shown for collagens and ECM glycoproteins. $^{*}p<0.05$, $^{**}p<0.01$, $^{***}p<0.001$, $^{****}p<0.0001$, and ns=not significant (p-value shown>0.05).

The relative distribution of different ECM proteins varies during overload. Although matrisome percentage did not significantly change, the type of matrisome was noticeably different throughout overload (Figure 3.6B). Immediately after injury, ECM glycoprotein content

significantly increased, while collagen content decreased (Figure 3.6C and Table 3.6). Throughout overload, the collagen content was restored similar to the non-injured plantaris muscle as the tissue returned to homeostasis. Aside from the ECM regulator percentage peak at day 2, other matrisome-associated classifications fluctuated with hypertrophy. Together, these results suggest that different types of ECM proteins are expressed throughout repair to facilitate the compensatory hypertrophy of the plantaris muscle.

Table 3.6: ECM classification percentages for overload proteomics.

Sample / **Classification**	0 Aha	2 Aha	7 Aha	14 Aha	28 Aha
Core Matrisome					
Collagens	94.05% ± 1.08%	75.79% ± 7.96%	83.57% ± 0.99%	85.01% ± 0.94%	89.03% ± 2.87%
Proteoglycans	1.70% ± 0.10%	1.45% ± 0.34%	2.53% ± 0.42%	3.02% ± 0.23%	3.55% ± 0.86%
ECM Glycoproteins	0.91% ± 0.20%	14.39% ± 5.30%	7.22% ± 2.32%	3.97% ± 0.08%	3.91% ± 1.34%
Matrisome-Associated					
ECM-Affiliated Proteins	2.68% ± 0.67%	3.72% ± 0.76%	5.27% ± 0.70%	6.01% ± 0.64%	2.99% ± 1.18%
ECM Regulators	0.66% ± 0.14%	4.13% ± 1.48%	1.34% ± 0.47%	1.90% ± 0.02%	0.49% ± 0.16%
Secreted Factors	0.01% ± 0.002%	0.52% ± 0.22%	0.06% ± 0.01%	0.08% ± 0.01%	0.03% ± 0.04%

Analysis of individual ECM proteins showed significant dynamics throughout overload. To identify the differential dynamics of individual ECM proteins throughout overload, row z-scores were calculated and visualized using heat maps grouped by classification (Figure 3.7). Core matrisome proteins are essential for structural functions in skeletal muscle and were more abundantly identified throughout the duration of overload than the matrisome-associated proteins. Collagens are the main structural component and are important in transmitting forces and maintaining the mechanical integrity of skeletal muscle tissue [36,37]. Interestingly, the relative abundance of type I collagen chains (COL1A1 and COL1A2) decreased over time, while types III (COL3A1) and V (COL5A1 and COL5A2), which are important for type I collagen fibrillogenesis [33,34], increased throughout the duration of overload. Type IV (COL4A1 and COL4A2) and type

VI (COL6A1 and COL6A2) collagens are important in basement membrane stability [36,37] and increased throughout overload.

Other key basement membrane proteins (NID1, LAMA2, LAMA4, LAMB1, LAMB2, and LAMC1) were included in a set of glycoproteins that also increased throughout overload [38,39]. The increase of basement membrane proteins correlate with the formation of blood vessels seen at later timepoints. Additionally, the main components of the basal lamina, type IV collagen and laminins, are important in muscle development by activating molecular signaling [39] and regulating satellite cell migration [40]. Interestingly, only LAMB2 showed a significant increase in relative protein abundance after 28 days. This suggests increased remodeling of neuromuscular junctions where the role of LAMB2 has been previously characterized [41]. A secondary set of glycoproteins were identified only during injury, indicating the need for other ECM components during these time points. These proteins decreased in abundance at different rates throughout overload and could be indicators of ECM remodeling. Another indicator of tissue remodeling was observed by the group of ECM regulators, such as inter-α-trypsin inhibitors (ITIH1, ITIH2, ITIH3, and ITIH4), that were exclusively identified at day 2. The ITI protein family has been shown to play a role in hyaluronic acid synthesis [42], which correlates with the increased deposition of hyaluronic acid observed in a previous plantaris muscle hypertrophy study [17].

A majority of the identified proteoglycans (*i.e.* FMOD, DCN, OGN, and LUM) decreased in abundance during the inflammatory stage and had greatest abundance after homeostasis was restored. Many small leucin-rich proteoglycans (SLRPs), which are important in growth factor signaling and collagen binding [43], had significant differences in abundance throughout overload and greatest abundance at the later stages of hypertrophy (ASPN, BGN, PRELP, LUM, and OGN). Periostin (POSTN) was differentially regulated and peaked intensity at 7 days, suggesting it is important during hypertrophy. Moreover, POSTN has been implicated to promote fibroblast migration in skeletal muscle injury and prevent scar formation [44].

Many of these individual protein trends are presented in Figure 3.8. Relative protein abundances were subjected to one-way ANOVA analysis to identify significant trends over time.

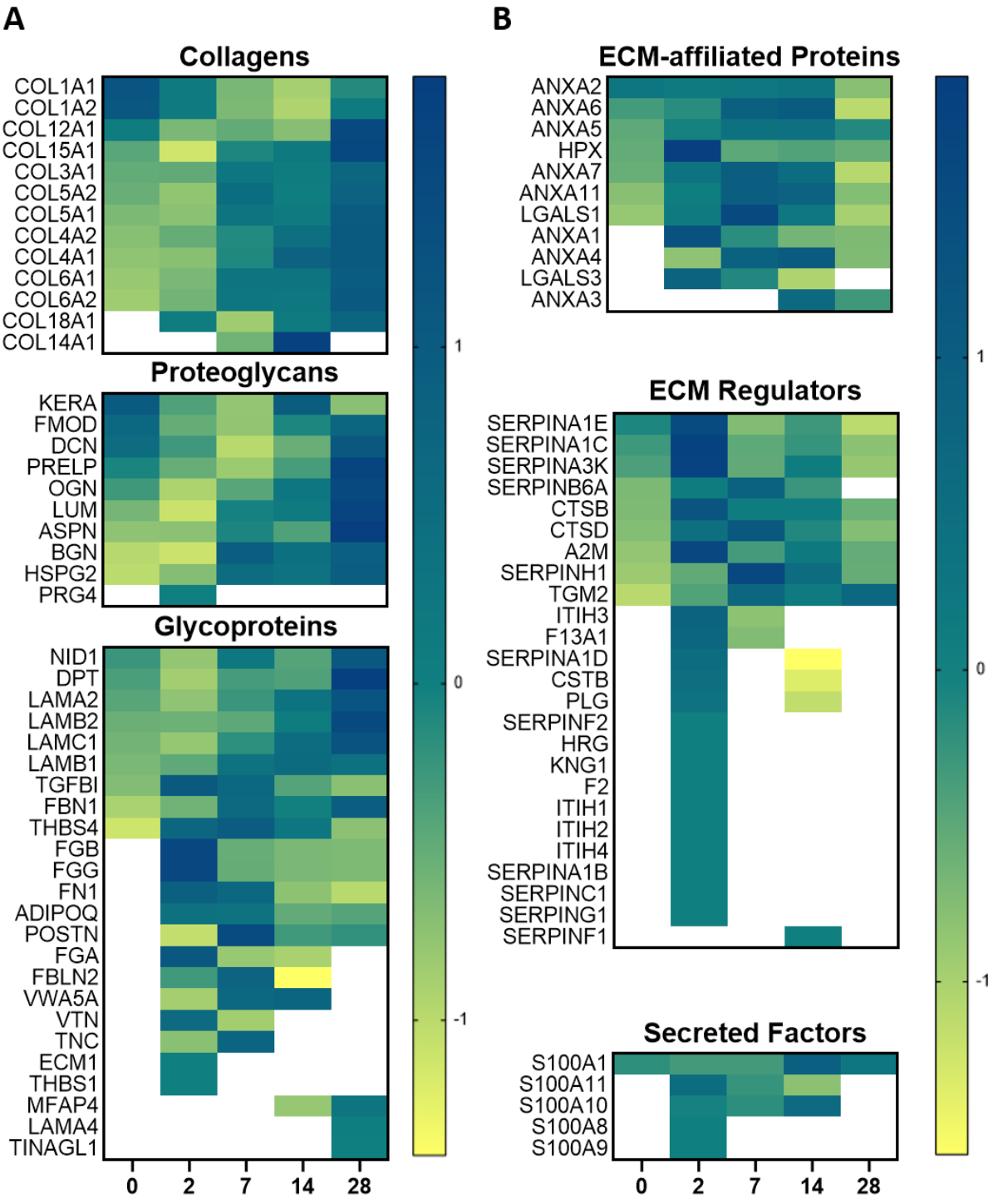

Figure 3.7: Row z-scores of matrisome proteins during overload. (A) Core matrisome and **(B)** matrisome-associated classifications of proteomic trends throughout overload. LFQ intensities were used to determine a row z-score for matrisome proteins. Data is shown as the average row z-score of non-zero values within 3 biological replicates for each time point (n=2 for 14 days).

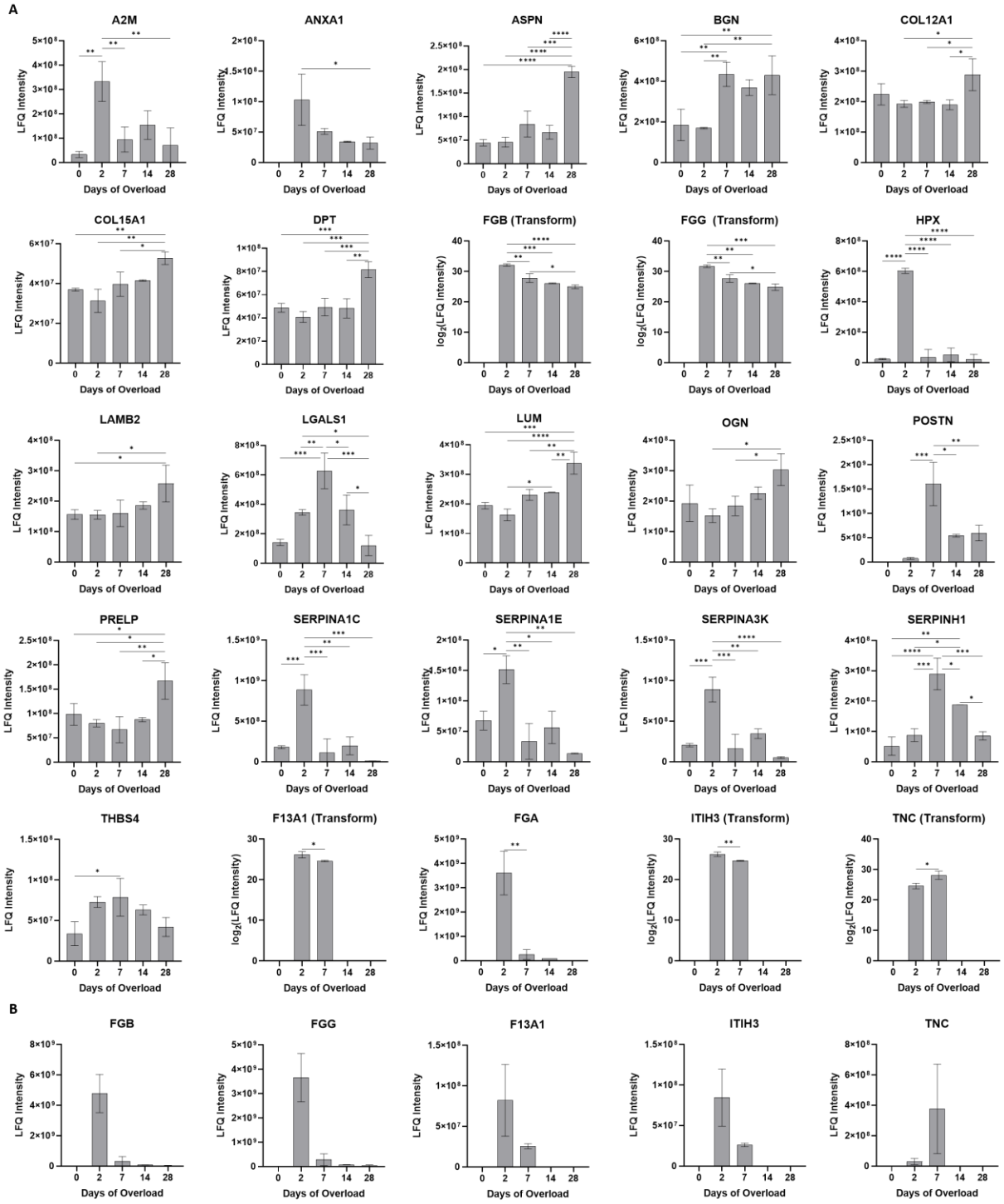

Figure 3.8: Matrisome proteins with significant trends throughout overload. (A) LFQ intensities within each protein were tested for normal distribution (Shapiro-Wilk test) and equal variance (Brown-Forsythe test) before being analyzed by one-way ANOVA. If either test was failed, but passed after $\log_2$ transformation, the transformed data was used to analyze the significance (noted in title). Proteins identified in only two time points were analyzed via t-test using similar assumption testing. **(B)** Original LFQ Intensity for transformed data. Each time point represents 3 biological replicates (n=2 for 14 days) and presented as a mean ± standard deviation.

Relative intensities of unenriched proteins from Aha-labeled plantaris muscle were similar to PBS controls. To confirm that Aha-labeled proteins do not alter LC-MS/MS results, non-injured plantaris muscle tissue was compared between Aha-injected and PBS-injected control mice. Tissues were directly analyzed by LC-MS/MS without undergoing the click reaction or neutravidin bead enrichment. The percentage of total raw intensity for every protein was calculated and corresponding values for PBS and Aha samples were plotted against each other (Figure 3.9). Overall, proteins had similar distributions in PBS and Aha tissues, indicating that the injections did not alter the unenriched composition of plantaris tissue. Although there were not many differences in protein distribution, there were more proteins exclusively identified in Aha-labeled muscles. However, this could be due to slight variations in sample preparation and LC-MS/MS, shown by an overall increase of the number of proteins identified in the Aha sample. Furthermore, unenriched proteins from all stages of hypertrophy must be evaluated to fully understand the impact of Aha-labeling on the proteome of injured adult muscle.

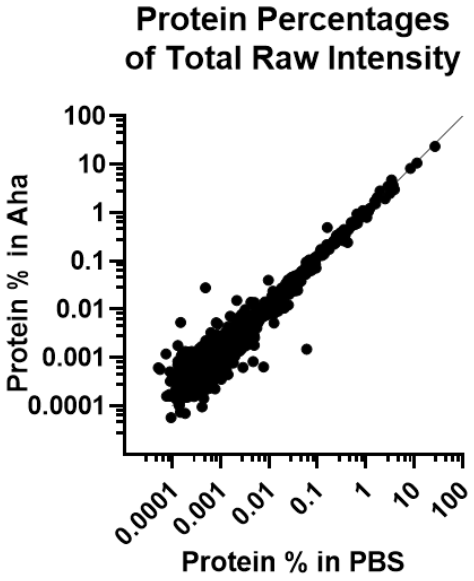

Figure 3.9: Comparison of protein intensities identified in PBS or Aha-injected tissues. The percentage of raw intensities were plot for each protein identified in both samples. Trendline slope=1.

3.4 Analysis of NSPs

BONCAT was successfully used to label NSPs in overloaded tissue. Cycloaddition click reactions between the azide in Aha-labeled proteins and biotin-alkyne, followed by western blot analysis, enabled visualization of NSPs in overloaded plantaris tissues (Figure 3.10). Plantaris muscles and aponeuroses from Aha-injected and control mice were harvested 6 hours post-injection. Soluble proteins from tissue samples were clicked with biotin-alkyne and analyzed via western blot. Membranes were probed with a fluorophore conjugated streptavidin and imaging revealed NSPs during different days of overload. Minimal fluorescence intensity in control tissues indicated low non-specific binding of biotin-alkyne during the click reaction. Notably, there was an increase of NSPs in injured Aha-labeled tissues, compared to non-injured tissue, suggesting a lower rate of protein synthesis in homeostatic tissue.

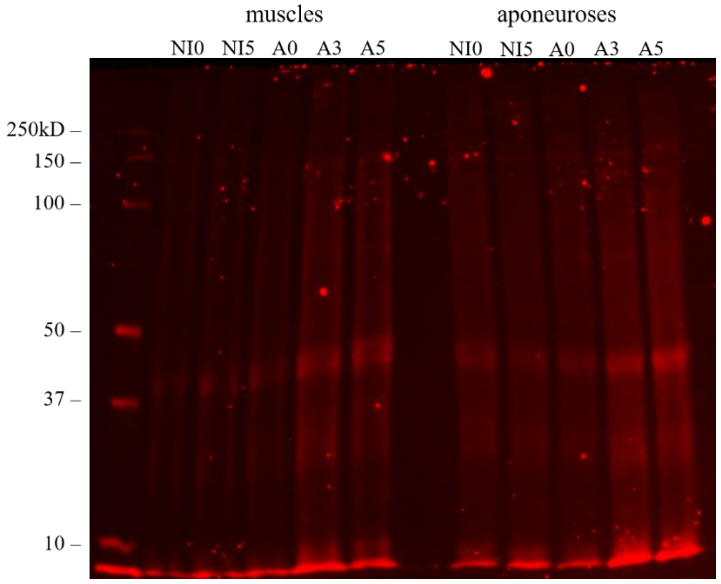

Figure 3.10: BONCAT fluorescent labeling in plantaris tissues. Each lane contained equal amount of protein within the muscle and aponeurosis groups. Fluorophore conjugated streptavidin identified biotinylated NSPs in both groups at 3 and 5 days of overload. Lanes: 1=ladder, 2-6=muscle tissue (M), 8-12=aponeurosis tissue. Labels: NI=non-injected mouse as control, A=Aha-injected mouse, #=days of overload.

Western blot reveals successful enrichment of NSPs from muscle tissue. To provide proof of concept that NSPs can be enriched from adult murine muscle, hindlimb muscle tissues were harvested from Aha or PBS injected mice and solubilized in 8M urea. The soluble protein and

remaining insoluble pellet were clicked with biotin-alkyne. Biotinylated NSPs were separated from tissue extracts using neutravidin beads. Western blot analysis revealed NSPs in Aha-labeled tissue (Figure 3.11). PBS background labeling was lower than Aha-labeled tissues. These results show that NSPs can be isolated from homeostatic skeletal muscle tissue.

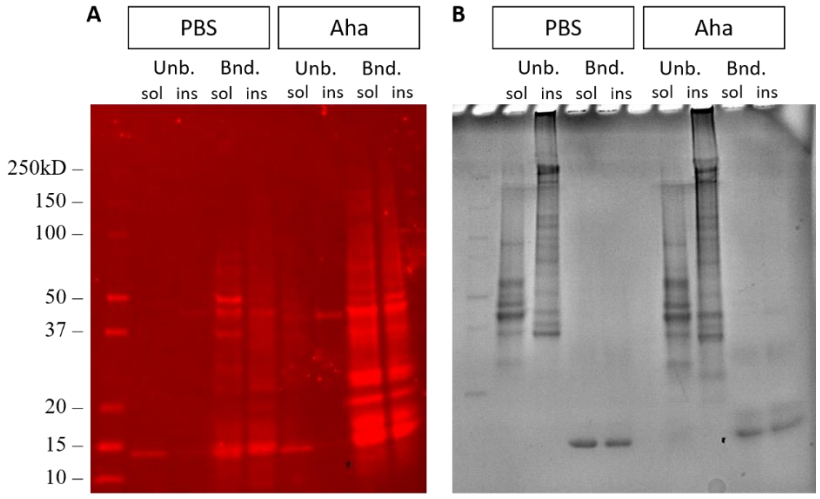

Figure 3.11: Aha enrichment of NSPs in uninjured skeletal muscle tissue. Murine hindlimb muscles were subject to 8M urea solubilization, clicked with biotin-alkyne, and enriched with neutravidin beads. **(A)** Fluorophore conjugated streptavidin probed NSPs, showing a larger signal to noise ratio in Aha-labeled tissue. **(B)** Gel Code Blue stained gel confirmed the presence of proteins in non-fluorescent lanes. Lanes: 1=ladder, 2-5=PBS-labeled tissue, 6-9=Aha-labeled tissue. Labels: Unb.=supernatant of unbound proteins from neutravidin enrichment, Bnd.=biotinylated proteins bound to beads in neutravidin enrichment, sol=8M urea solubilized proteins, ins=insoluble proteins.

It is expected that the neutravidin enrichment will successfully isolate the NSPs at each time point of overload. The increase of fluorescent intensity in Aha-labeled and injured plantaris muscles suggest that there will be an increase in signal to noise ratio in the Aha enrichment of overloaded tissues.

CHAPTER 4. DISCUSSION

Skeletal muscle injuries that cause VML have limited repair and regenerative capabilities due fibrosis, the increased deposition of ECM [3]. The ECM has been shown to facilitate muscle growth [4-6], but current treatments fail to restore functional tissue due to limited knowledge of source matrix and signaling molecules [7]. Recently, researchers have studied the ECM during muscle growth, while few studies have evaluated only a handful of ECM proteins during skeletal muscle hypertrophy [17,18]. In this study, compensatory hypertrophy of the murine plantaris muscle was used with LC-MS/MS to obtain a global analysis of ECM dynamics during tissue repair and restoration. With these methods, we were able to identify specific trends of signaling molecules and provide knowledge of source matrix throughout muscle growth that tissue engineers can use to promote the development of successful regenerative therapies.

Initial injuries were performed by an Achilles tenectomy, but poor overload of the plantaris suggested synergistic ablation was necessary. Following the surgical removal of the gastrocnemius and soleus muscles, we observed a general increase in the plantaris mass ratio throughout overload with a slight drop between 7 and 14 days. This could be due to the initial increase of muscle mass caused by surgical trauma which peaks at 5 days and becomes negligible after 16 days [10]. Additionally, variability in plantaris muscle mass was observed due to difficulty in harvesting at later timepoints of hypertrophy, as dense connective tissues formed around the muscle. Overall, a significant increase of the plantaris muscle mass was observed at 28 days resulting in a 40% mass increase, similar to other studies that use this injury model in rats [45]. Although we referred to 28 days as the restoration of homeostasis, it is assumed that plantaris muscle mass increases and the ECM continues to remodel after this time point.

LC-MS/MS enabled a global quantitative analysis of ECM proteins throughout stages of hypertrophy. Although our lab has previously adapted a tissue fractionation technique to extract intracellular proteins and isolate the matrisome prior to mass spectrometry, we found that the fractionation of adult tissues did not hold the benefits of those in embryonic tissues [26,31]. Using 8M urea to solubilize uninjured plantaris tissues, over 100 ECM proteins were identified by LC-MS/MS. In general, LC-MS/MS is limited by the length of time proteins are resolved over,

potentially preventing identification of ECM proteins of low abundance critical for hypertrophy. Our results showed a significant increase in the relative intensity of muscle specific proteins of low abundance after removing the aponeurosis. In addition, false-positive recognition of ECM proteins highly expressed in tendon was limited after removing the aponeurosis, an ECM-rich tendon mass. Future studies that utilize this model to study the ECM composition and turnover are advised to remove the aponeurosis to limit LC-MS/MS interference.

Utilizing the injury model and LC-MS/MS techniques in tandem identified a global analysis of ECM protein dynamics throughout overload which revealed 25 significant trends. Overall, there was a significant decrease in the relative abundance of collagen and a significant increase in the relative abundance of glycoproteins during the initial inflammatory response. Type I collagen (COL1A1 and COL1A2) showed a general decrease throughout injury similar to the significant decrease observed in a previously studied follistatin-induced skeletal muscle hypertrophy model [24]. Notably, both collagens important in type I collagen fibrillogenesis, types III (COL3A1) and V (COL5A1 and COL5A2), increased throughout overload. While an increase of type III collagen has been characterized during skeletal muscle healing [46], trends of type V collagen during repair have not yet been clearly identified [47]. Notably, only COL12A1 and COL15A1 showed a significant increase as a results of compensatory hypertrophy while a previous study identify a significant increase in the gene expression of multiple additional collagens [18].

When identifying proteins specific to the basement membrane (COL4A1, COL4A2, COL6A1, COL6A2, NID1, LAMA2, LAMA4, LAMB1, LAMB2, and LAMC1), a similar increase was observed throughout overload. These results further indicate the importance of the basement membrane and basal lamina during skeletal muscle development and repair [39], [40]. Interestingly, only LAMB2 showed a significant increase in relative abundance after 28 days. On the contrary, a previous study that induced skeletal muscle injury via cardiotoxin injection concluded the relative expression of *Lama2, Lama4, Lamb1, and Lamc1* significantly increased while the expression of *Lamb2* was unchanged [40]. These differences indicate potential ECM remodeling cues important for either repair or regeneration.

Many significant trends determined within this study have previously been shown in the two studies that have evaluated ECM remodeling following compensatory hypertrophy, [17] and [18], including: ASPN, BGN, COL12A1, COL15A1, LUM, and TNC. In addition, we identified new trends of proteins that have yet to be specifically characterized in skeletal muscle hypertrophy. POSTN was differentially regulated and had a peak intensity at 7 days, suggesting it is important in initiating hypertrophy. Furthermore, research has shown that POSTN promotes fibroblast migration and prevent scar formation after skeletal muscle injury [44]. The data must be further investigated to understand individual protein dynamics that have not been investigated in the literature.

A brief analysis of NSPs show the capability of BONCAT and neutravidin enrichment can be used on overloaded plantaris muscles. Western blot confirmed the increase of NSPs in Aha-labeled injured tissues when compared to both Aha-labeled uninjured tissues and non-injected controls. Furthermore, the enrichment of NSPs from uninjured muscle tissue provided a proof of concept of enrichment capabilities in adult tissue. Future work will be done to optimize these techniques and use LC-MS/MS to identify NSPs throughout different stages of hypertrophy. Providing the temporal distribution of protein synthesis will enhance our current knowledge of differential protein abundance as a function of hypertrophy.

In conclusion, we were able to identify key dynamics of ECM proteins during skeletal muscle hypertrophy. A global proteomic analysis was completed on overloaded plantaris muscles during multiple time points of injury and repair. Although the distinct influence of proteins was not evaluated, our identified proteomic trends show specific proteins that may play a key role during muscle development. These results give a better idea of potential knockout models that can be used to understand the specific role of different proteins. Furthermore, we identified source matrix and signaling molecules that increase in relative protein abundance during muscle growth. Ultimately, our study provides information of protein dynamics crucial for skeletal muscle tissue growth and repair. Tissue engineers can use these results to develop successful regenerative therapies and promote restoration to functional muscle tissue in severe injuries resulting in volumetric muscle loss.

APPENDIX A. MAXQUANT PARAMETERS

Table A.1: MaxQuant parameters for pre-injury proteomics.

Pre-injury Proteomics					
Parameter	**P SOL**	**T SOL**	**M SOL**	**T INS**	**M INS**
General					
Instrument type	Lumos				
MaxQuant Version	1.6.1.0				
Group	0			1	
Fraction	1	4	7	10	13
	Note: Fractions were set such that match between runs was enabled between biological replicates.				
LC-MS run type	Standard				
Multiplicity	1				
Labels	N/A				
Digestion					
Enzyme mode	Specific				
Enzymes	LysC, Trypsin				
Maximum missed cleavages	2				
Separate enzyme for first search	FALSE				
Modifications					
Fixed modifications	Carbamidomethyl on Cys (+57.012)				
Variable modifications	Oxidation of Met (+15.995 Da)				
	Deamidation of Asn (+0.984 Da)				
	Conversion of Gln to pyro-Glu (-17.027 Da)				
	Hydroxylysine (+15.995 Da)				
	Hydroxyproline (+15.995 Da)				
Maximum number of modifications per peptide	5				
Separate variable modifications for first search	FALSE				
Sequences					
Fasta files	Uniprot *Mus musculus* (December 2019)				
Include contaminants	TRUE				
Decoy mode	Revert				
Special AAs	FALSE				

Minimum peptide length	7
Maximum peptide mass	4600 Da
Minimum peptide length for unspecific search	8
Maximum peptide length for unspecific search	25
Identification	
PSM FDR	0.01
Protein FDR	0.01
Site FDR	0.01
Minimum unique peptides	0
Minimum razor + unique peptides	1
Minimum peptides	1
Minimum score for unmodified peptides	0
Minimum score for modified peptides	40
Minimum delta score for unmodified peptides	0
Minimum delta score for modified peptides	6
Main search maximum combinations	200
Base FDR calculations on delta score	FALSE
Razor protein FDR	TRUE
Second peptides	TRUE
Find dependent peptides	FALSE
Match between runs	TRUE
Labeled amino acid filtering	FALSE
Quantification	
Use only unmodified peptides	TRUE
Modifications included in protein quantification	Oxidation of Met (+15.995 Da)
	Deamidation of Asn (+0.984 Da)
	Conversion of Gln to pyro-Glu (-17.027 Da)
	Hydroxylysine (+15.995 Da)
	Hydroxyproline (+15.995 Da)
Peptides used for protein quantification	Unique + razor
Discard unmodified counterpart peptides	TRUE
Label minimum ratio count	2
Label-free quantification	TRUE
LFQ min. ratio count	2
Fast LFQ	TRUE
Separate LFQ in parameter groups	TRUE
Stabilize large LFQ ratios	TRUE
Require MS/MS for LFQ comparisons	TRUE

LFQ norm for sites and peptides	FALSE
iBAQ	TRUE
iBAQ log fit	TRUE
Re-quantify	FALSE
Advanced ratio estimation	FALSE

Table A.2: MaxQuant parameters for overload proteomics.

Overload Proteomics						
Parameter	**0 PBS**	**0 Aha**	**2 Aha**	**7 Aha**	**14 Aha**	**28 Aha**
General						
Instrument type	QE					
MaxQuant Version	1.6.7.0					
Group	0					
Fraction	1	4	7	10	13	16
	Note: Fractions were set such that match between runs was enabled between biological replicates.					
LC-MS run type	Standard					
Multiplicity	1					
Labels	N/A					
Digestion						
Enzyme mode	Specific					
Enzymes	LysC, Trypsin					
Maximum missed cleavages	2					
Separate enzyme for first search	FALSE					
Modifications						
Fixed modifications	Carbamidomethyl on Cys (+57.012)					
Variable modifications	Oxidation of Met (+15.995 Da)					
	Deamidation of Asn (+0.984 Da)					
	Hydroxylysine (+15.995 Da)					
	Hydroxyproline (+15.995 Da)					
	Met replacement by Aha (-4.986Da)					
Maximum number of modifications per peptide	5					
Separate variable modifications for first search	FALSE					
Sequences						
Fasta files	Uniprot *Mus musculus* (December 2019)					

Include contaminants	TRUE
Decoy mode	Revert
Special AAs	FALSE
Epsilon score for mutations	TRUE
Evaluate variant peptides separately	TRUE
Minimum peptide length	7
Maximum peptide mass	4600 Da
Minimum peptide length for unspecific search	8
Maximum peptide length for unspecific search	25
Identification	
PSM FDR	0.01
Protein FDR	0.01
Site FDR	0.01
Minimum unique peptides	0
Minimum razor + unique peptides	1
Minimum peptides	1
Minimum score for unmodified peptides	0
Minimum score for modified peptides	40
Minimum delta score for unmodified peptides	0
Minimum delta score for modified peptides	6
Main search maximum combinations	200
Base FDR calculations on delta score	FALSE
Razor protein FDR	TRUE
Second peptides	TRUE
Find dependent peptides	FALSE
Match between runs	TRUE
Labeled amino acid filtering	FALSE
Quantification	
Use only unmodified peptides	TRUE
Modifications included in protein quantification	Oxidation of Met (+15.995 Da)
	Deamidation of Asn (+0.984 Da)
	Hydroxylysine (+15.995 Da)
	Hydroxyproline (+15.995 Da)
	Met replacement by Aha (-4.986Da)
Peptides used for protein quantification	Unique + razor
Discard unmodified counterpart peptides	TRUE
Label minimum ratio count	2
Label-free quantification	TRUE

LFQ min. ratio count	2
Fast LFQ	TRUE
Separate LFQ in parameter groups	FALSE
Stabilize large LFQ ratios	TRUE
Require MS/MS for LFQ comparisons	TRUE
LFQ norm for sites and peptides	FALSE
iBAQ	TRUE
iBAQ log fit	TRUE
Re-quantify	FALSE
Advanced ratio estimation	FALSE

APPENDIX B. ECM PROTEIN INTENSITIES

Table B.1: Raw and LFQ intensities of matrisome proteins identified in overload proteomics. Data represented as average of non-zero values for three biological replicates (n=2 for 14 days).

Protein	Category	Classification	0 days		2 days		7 days		14 days		28 days	
			RAW	LFQ	RAW	LFQ	RAW	LFQ	RAW	LFQ	RAW	LFQ
ADIPOQ	Core	Glycoprotein	5.467E+06		2.186E+07	2.440E+07	1.141E+07	2.430E+07	2.770E+07	1.988E+07	4.717E+07	2.028E+07
SERPINA1B	Associated	Regulator			1.631E+07	1.294E+07						
SERPINA1C	Associated	Regulator	2.238E+08	1.781E+08	1.203E+09	8.852E+08	1.019E+08	1.077E+08	2.522E+08	1.958E+08	1.468E+07	9.008E+06
SERPINA1D	Associated	Regulator			1.628E+08	1.079E+08			7.433E+06	2.045E+07		
SERPINA1E	Associated	Regulator	7.319E+07	6.751E+07	2.107E+08	1.514E+08	1.934E+07	3.337E+07	5.358E+07	5.631E+07	8.899E+06	1.362E+07
SERPINF2	Associated	Regulator			5.354E+07	4.236E+07						
A2M	Associated	Regulator	2.231E+07	3.251E+07	4.233E+08	3.324E+08	1.193E+08	9.428E+07	1.666E+08	1.534E+08	6.698E+07	6.967E+07
ANXA1	Associated	Affiliated	6.107E+06		1.571E+08	1.031E+08	5.865E+07	5.101E+07	2.739E+07	3.433E+07	2.386E+07	3.190E+07
ANXA11	Associated	Affiliated	7.690E+07	8.808E+07	1.549E+08	1.044E+08	1.866E+08	1.242E+08	1.292E+08	1.214E+08	9.092E+07	8.869E+07
ANXA2	Associated	Affiliated	1.860E+09	1.795E+09	2.251E+09	1.775E+09	2.206E+09	1.790E+09	1.900E+09	1.804E+09	1.963E+09	1.665E+09
ANXA3	Associated	Affiliated			9.031E+06		5.953E+06		9.047E+06	1.130E+07	9.009E+06	8.707E+06
ANXA4	Associated	Affiliated	1.051E+06		2.232E+07	1.976E+07	4.539E+07	3.438E+07	3.539E+07	3.602E+07	2.083E+07	2.062E+07
ANXA5	Associated	Affiliated	3.174E+08	3.201E+08	3.254E+08	3.471E+08	4.623E+08	3.718E+08	4.172E+08	3.729E+08	4.375E+08	3.421E+08
ANXA6	Associated	Affiliated	6.981E+08	6.894E+08	9.232E+08	7.265E+08	1.177E+09	9.423E+08	9.961E+08	9.754E+08	5.904E+08	5.330E+08
ANXA7	Associated	Affiliated	4.297E+07	5.987E+07	9.635E+07	7.307E+07	1.272E+08	8.209E+07	8.574E+07	7.578E+07	5.187E+07	5.252E+07
SERPINC1	Associated	Regulator	3.057E+06		1.533E+07	1.221E+07	2.777E+06		4.121E+06		5.555E+06	
ASPN	Core	Proteoglycan	3.645E+07	4.457E+07	4.027E+07	4.571E+07	9.860E+07	8.408E+07	3.428E+07	6.664E+07	3.040E+08	1.945E+08
HSPG2	Core	Proteoglycan	2.573E+08	3.010E+08	3.557E+08	3.381E+08	6.790E+08	4.789E+08	4.688E+08	4.588E+08	7.290E+08	5.243E+08
BGN	Core	Proteoglycan	1.960E+08	1.851E+08	2.039E+08	1.696E+08	5.568E+08	4.346E+08	3.537E+08	3.697E+08	5.883E+08	4.304E+08
PRG2	Core	Proteoglycan			1.919E+07							
CTSB	Associated	Regulator	1.959E+07	2.465E+07	1.104E+08	5.828E+07	3.782E+07	3.847E+07	2.003E+07	3.810E+07	2.179E+07	2.689E+07
CTSD	Associated	Regulator	1.064E+08	9.484E+07	1.508E+08	1.332E+08	1.432E+08	1.549E+08	1.405E+08	1.150E+08	1.132E+08	9.485E+07
CTSZ	Associated	Regulator	1.017E+07		9.379E+06		1.323E+07		8.291E+06		7.892E+06	
F13A1	Associated	Regulator			1.122E+08	8.222E+07	2.286E+07	2.549E+07				
COL1A1	Core	Collagen	7.144E+10	4.433E+10	6.357E+10	3.281E+10	4.641E+10	2.491E+10	3.112E+10	2.213E+10	6.232E+10	3.012E+10
COL2A1	Core	Collagen							5.432E+06		1.523E+07	
COL3A1	Core	Collagen	3.870E+09	2.890E+09	4.508E+09	2.903E+09	6.627E+09	4.179E+09	5.200E+09	3.829E+09	8.800E+09	4.965E+09
COL4A1	Core	Collagen	2.805E+07	3.472E+07	5.278E+07	3.629E+07	4.358E+07	5.381E+07	7.034E+07	7.958E+07	1.389E+08	8.669E+07

COL5A1	Core	Collagen	8.590E+07	8.022E+07	9.780E+07	7.614E+07	1.492E+08	1.217E+08	1.195E+08	1.134E+08	2.058E+08	1.532E+08
COL6A1	Core	Collagen	3.591E+08	3.995E+08	5.170E+08	4.578E+08	9.974E+08	7.774E+08	7.252E+08	7.655E+08	1.394E+09	1.002E+09
COL11A1	Core	Collagen	4.523E+07		5.544E+07				3.490E+07		1.058E+07	
COL12A1	Core	Collagen	2.166E+08	2.242E+08	2.179E+08	1.927E+08	2.418E+08	1.992E+08	1.732E+08	1.895E+08	4.620E+08	2.888E+08
COL14A1	Core	Collagen					1.552E+07	1.334E+07	1.674E+07	2.872E+07	3.826E+06	
COL15A1	Core	Collagen	4.955E+07	3.687E+07	4.351E+07	3.128E+07	4.334E+07	3.963E+07	3.677E+07	4.150E+07	5.656E+07	5.270E+07
COL18A1	Core	Collagen	1.188E+07		2.558E+07	1.930E+07	1.880E+07	1.559E+07	2.067E+07	1.969E+07	2.782E+07	2.224E+07
COL1A2	Core	Collagen	4.255E+10	3.236E+10	3.796E+10	2.495E+10	2.782E+10	1.945E+10	2.013E+10	1.728E+10	4.006E+10	2.492E+10
COL4A2	Core	Collagen	3.846E+07	4.751E+07	4.821E+07	5.498E+07	9.956E+07	6.909E+07	9.079E+07	8.932E+07	1.559E+08	1.117E+08
COL5A2	Core	Collagen	1.178E+08	1.133E+08	1.342E+08	9.984E+07	2.403E+08	1.689E+08	1.172E+08	1.429E+08	2.853E+08	1.857E+08
COL6A2	Core	Collagen	1.399E+08	1.863E+08	2.561E+08	2.304E+08	5.066E+08	3.704E+08	3.366E+08	3.638E+08	7.866E+08	5.102E+08
CSTB	Associated	Regulator			4.010E+07	2.981E+07			9.664E+06	1.015E+07		
CST3	Associated	Regulator	1.092E+07		7.288E+06		5.831E+06				7.005E+06	
DCN	Core	Proteoglycan	5.832E+08	4.788E+08	5.290E+08	3.663E+08	3.031E+08	2.676E+08	3.191E+08	3.320E+08	8.161E+08	5.546E+08
DPT	Core	Glycoprotein	4.555E+07	4.878E+07	1.767E+07	4.087E+07	6.375E+07	4.932E+07	5.400E+07	4.828E+07	1.370E+08	8.159E+07
CTSC	Associated	Regulator			1.293E+07		8.558E+06		4.778E+06			
ECM1	Core	Glycoprotein			9.263E+06	8.614E+06						
FBN1	Core	Glycoprotein	1.841E+08	3.012E+08	5.243E+08	4.325E+08	1.342E+09	8.875E+08	6.131E+08	6.478E+08	1.627E+09	1.009E+09
FGA	Core	Glycoprotein			4.834E+09	3.601E+09	2.427E+08	2.464E+08	3.915E+07	8.540E+07	6.717E+06	
FGB	Core	Glycoprotein	3.791E+06		6.426E+09	4.775E+09	5.088E+08	3.245E+08	6.488E+07	7.339E+07	2.967E+07	3.478E+07
FGG	Core	Glycoprotein	5.685E+06		4.967E+09	3.659E+09	3.643E+08	2.787E+08	7.501E+07	7.134E+07	3.200E+07	3.606E+07
FMOD	Core	Proteoglycan	4.185E+08	4.039E+08	3.631E+08	2.807E+08	2.967E+08	2.527E+08	3.322E+08	3.262E+08	5.309E+08	4.083E+08
FN1	Core	Glycoprotein	4.443E+06		1.352E+09	9.671E+08	1.200E+09	8.738E+08	1.902E+08	3.322E+08	1.481E+08	2.358E+08
FBLN2	Core	Glycoprotein			1.561E+07	1.275E+07	2.514E+07	1.968E+07	4.868E+06	5.455E+06		
FBLN5	Core	Glycoprotein							1.995E+06		9.024E+06	
LGALS3	Associated	Affiliated			5.433E+07	6.030E+07	7.420E+07	4.083E+07	1.496E+07	2.147E+07		
LGALS1	Associated	Affiliated	1.192E+08	1.414E+08	4.493E+08	3.450E+08	7.871E+08	6.267E+08	3.762E+08	3.613E+08	1.238E+08	1.201E+08
HPX	Associated	Affiliated	4.069E+07	2.313E+07	7.270E+08	6.040E+08	3.651E+07	3.514E+07	8.472E+07	5.097E+07	1.414E+07	2.080E+07
HRG	Associated	Regulator			4.940E+07	3.924E+07						
ITIH4	Associated	Regulator			1.039E+08	8.332E+07						
ITIH1	Associated	Regulator			8.014E+07	6.120E+07						
ITIH2	Associated	Regulator			6.137E+07	4.866E+07	4.146E+06					
ITIH3	Associated	Regulator			1.241E+08	8.451E+07	1.258E+07	2.624E+07	3.158E+06			
KERA	Core	Proteoglycan	8.565E+07	6.234E+07	5.489E+07	4.121E+07	1.972E+07	3.516E+07	4.808E+07	6.161E+07	4.997E+07	3.596E+07
KNG1	Associated	Regulator	2.699E+06		1.477E+08	1.014E+08	4.949E+06		2.680E+06			
LAMA2	Core	Glycoprotein	2.044E+08	2.112E+08	2.032E+08	1.903E+08	1.888E+08	2.222E+08	2.509E+08	2.586E+08	5.348E+08	3.146E+08
LAMA4	Core	Glycoprotein			2.254E+06		3.329E+06		9.781E+06		1.056E+07	1.050E+07

LAMB1	Core	Glycoprotein	7.589E+07	6.788E+07	6.394E+07	7.136E+07	1.024E+08	8.834E+07	1.060E+08	9.226E+07	9.314E+07	8.878E+07
LAMB2	Core	Glycoprotein	1.590E+08	1.560E+08	1.930E+08	1.552E+08	1.772E+08	1.600E+08	1.737E+08	1.857E+08	3.661E+08	2.579E+08
LAMC1	Core	Glycoprotein	1.647E+08	1.983E+08	1.682E+08	1.835E+08	2.456E+08	2.277E+08	3.155E+08	2.752E+08	5.164E+08	3.291E+08
LUM	Core	Proteoglycan	1.986E+08	1.942E+08	1.719E+08	1.630E+08	2.499E+08	2.305E+08	2.282E+08	2.392E+08	5.022E+08	3.377E+08
MFAP4	Core	Glycoprotein			7.170E+06				6.636E+06	9.133E+06	2.564E+07	1.992E+07
OGN	Core	Proteoglycan	2.130E+08	1.930E+08	1.685E+08	1.524E+08	2.223E+08	1.839E+08	2.084E+08	2.263E+08	3.948E+08	3.036E+08
NID1	Core	Glycoprotein	1.557E+08	1.685E+08	1.555E+08	1.519E+08	2.483E+08	1.831E+08	1.571E+08	1.636E+08	2.952E+08	2.107E+08
NID2	Core	Glycoprotein					7.433E+06		1.717E+07			
POSTN	Core	Glycoprotein			5.671E+07	7.162E+07	2.030E+09	1.602E+09	5.049E+08	5.389E+08	7.283E+08	5.941E+08
SERPINF1	Associated	Regulator							1.255E+07	1.366E+07		
SERPING1	Associated	Regulator			1.004E+07	8.285E+06						
PLG	Associated	Regulator			1.116E+09	8.545E+08	5.299E+06		1.300E+07	1.404E+07		
PRELP	Core	Proteoglycan	1.107E+08	9.813E+07	8.599E+07	7.983E+07	4.266E+07	6.668E+07	6.115E+07	8.734E+07	2.819E+08	1.668E+08
LMAN1	Associated	Affiliated					9.567E+06					
S100A1	Associated	Secreted	1.300E+07	1.441E+07	1.479E+07	1.326E+07	1.545E+07	1.327E+07	2.541E+07	2.469E+07	2.442E+07	1.844E+07
S100A10	Associated	Secreted	5.601E+06		1.360E+07	1.193E+07	1.351E+07	1.153E+07	8.225E+06	1.362E+07		
S100A11	Associated	Secreted			4.522E+07	3.764E+07	3.250E+07	2.875E+07	2.020E+07	2.236E+07		
S100A8	Associated	Secreted			3.078E+08	2.294E+08						
S100A9	Associated	Secreted			3.273E+08	2.536E+08					9.042E+06	
TGM2	Associated	Regulator	4.041E+07	6.036E+07	8.742E+07	8.003E+07	1.754E+08	1.140E+08	8.528E+07	9.674E+07	1.653E+08	1.134E+08
PRG4	Core	Proteoglycan			1.700E+07	1.345E+07						
F2	Associated	Regulator			2.082E+07	1.646E+07						
SERPINA3K	Associated	Regulator	2.057E+08	2.048E+08	1.207E+09	8.901E+08	1.622E+08	1.611E+08	3.060E+08	3.458E+08	5.401E+07	5.103E+07
SERPINB6A	Associated	Regulator	2.094E+07	2.641E+07	7.174E+07	4.763E+07	1.050E+08	7.133E+07	2.664E+07	3.874E+07	6.931E+06	
SERPINH1	Associated	Regulator	4.202E+07	5.160E+07	1.013E+08	8.789E+07	3.615E+08	2.895E+08	2.015E+08	1.876E+08	9.004E+07	8.561E+07
SPARC	Core	Glycoprotein							9.640E+06			
TNC	Core	Glycoprotein	2.424E+06		2.690E+07	2.938E+07	4.559E+08	3.764E+08				
THBS1	Core	Glycoprotein			6.317E+07	5.042E+07						
THBS4	Core	Glycoprotein	2.031E+07	3.375E+07	1.177E+08	7.283E+07	1.028E+08	7.877E+07	5.423E+07	6.308E+07	4.043E+07	4.211E+07
TGFBI	Core	Glycoprotein	5.262E+07	5.912E+07	1.248E+08	8.057E+07	9.717E+07	7.561E+07	4.694E+07	6.254E+07	7.252E+07	5.854E+07
TINAGL1	Core	Glycoprotein	3.595E+06		5.181E+06						1.198E+07	1.030E+07
VCAN	Core	Proteoglycan	1.787E+07				4.353E+06				7.119E+06	
VTN	Core	Glycoprotein			4.880E+08	3.807E+08	8.185E+06	1.019E+07				
VWA5A	Core	Glycoprotein			1.107E+07	1.273E+07	2.879E+07	1.658E+07	1.306E+07	1.680E+07		

REFERENCES

[1] S. M. Greising, B. T. Corona, C. McGann, J. K. Frankum, and G. L. Warren, "Therapeutic Approaches for Volumetric Muscle Loss Injury: A Systematic Review and Meta-Analysis," *Tissue Engineering - Part B: Reviews*, vol. 25, no. 6. Mary Ann Liebert Inc., pp. 510–525, 01-Dec-2019.

[2] C. J. Mann *et al.*, "Aberrant repair and fibrosis development in skeletal muscle," *Skelet. Muscle*, vol. 1, no. 1, p. 21, 2011.

[3] B. T. Corona, J. C. Rivera, and S. M. Greising, "Inflammatory and Physiological Consequences of Debridement of Fibrous Tissue after Volumetric Muscle Loss Injury," *Clin. Transl. Sci.*, vol. 11, no. 2, pp. 208–217, Mar. 2018.

[4] S. C. Goetsch, T. J. Hawke, T. D. Gallardo, J. A. Richardson, and D. J. Garry, "Transcriptional profiling and regulation of the extracellular matrix during muscle regeneration," *Physiol. Genomics*, vol. 14, pp. 261–271, 2003.

[5] A. L. Serrano and P. Muñoz-Cánoves, "Regulation and dysregulation of fibrosis in skeletal muscle," *Experimental Cell Research*, vol. 316, no. 18. Academic Press Inc., pp. 3050–3058, 01-Nov-2010.

[6] N. Osses and E. Brandan, "ECM is required for skeletal muscle differentiation independently of muscle regulatory factor expression," *Am. J. Physiol. - Cell Physiol.*, vol. 282, no. 2 51-2, 2002.

[7] T. L. Sarrafian, S. C. Bodine, B. Murphy, J. K. Grayson, and S. M. Stover, "Extracellular matrix scaffolds for treatment of large volume muscle injuries: A review," *Veterinary Surgery*, vol. 47, no. 4. Blackwell Publishing Inc., pp. 524–535, 01-May-2018.

[8] D. A. Lowe and S. E. Alway, "Animal Models for Inducing Muscle Hypertrophy: Are They Relevant for Clinical Applications in Humans?," 2002.

[9] A. L. Goldberg, "Work-induced growth of skeletal muscle in normal and hypophysectomized rats.," *Am. J. Physiol.*, vol. 213, no. 5, pp. 1193–1198, 1967.

[10] R. B. Armstrong, P. Marum, P. Tullson, and C. W. Saubert IV, "Acute hypertrophic response of skeletal muscle to removal of synergists," *J. Appl. Physiol. Respir. Environ. Exerc. Physiol.*, vol. 46, no. 4, pp. 835–842, 1979.

[11] D. M. DiPasquale *et al.*, "Urokinase-type plasminogen activator and macrophages are

required for skeletal muscle hypertrophy in mice," *Am. J. Physiol. Physiol.*, vol. 293, no. 4, pp. C1278–C1285, Oct. 2007.

[12] C. M. Westerkamp and S. E. Gordon, "Angiotensin-converting enzyme inhibition attenuates myonuclear addition in overloaded slow-twitch skeletal muscle," *Am. J. Physiol. Integr. Comp. Physiol.*, vol. 289, no. 4, pp. R1223–R1231, Oct. 2005.

[13] C. S. Fry *et al.*, "Regulation of the muscle fiber microenvironment by activated satellite cells during hypertrophy," *FASEB J.*, vol. 28, no. 4, pp. 1654–1665, 2014.

[14] C. S. Fry, T. J. Kirby, K. Kosmac, J. J. McCarthy, and C. A. Peterson, "Myogenic Progenitor Cells Control Extracellular Matrix Production by Fibroblasts during Skeletal Muscle Hypertrophy," *Cell Stem Cell*, vol. 20, no. 1, pp. 56–69, Jan. 2017.

[15] J. J. McCarthy and K. A. Esser, "MicroRNA-1 and microRNA-133a expression are decreased during skeletal muscle hypertrophy," *J. Appl. Physiol.*, vol. 102, no. 1, pp. 306–313, Jan. 2007.

[16] M. Miyazaki and K. A. Esser, "Cellular mechanisms regulating protein synthesis and skeletal muscle hypertrophy in animals," *J. Appl. Physiol.*, vol. 106, no. 4, pp. 1367–1373, Apr. 2009.

[17] S. Calve, J. Isaac, J. P. Gumucio, and C. L. Mendias, "Hyaluronic acid, HAS1, and HAS2 are significantly upregulated during muscle hypertrophy," *Am. J. Physiol. Physiol.*, vol. 303, no. 5, pp. C577–C588, Sep. 2012.

[18] C. L. Mendias, A. J. Schwartz, J. A. Grekin, J. P. Gumucio, and K. B. Sugg, "Changes in muscle fiber contractility and extracellular matrix production during skeletal muscle hypertrophy," *J. Appl. Physiol.*, vol. 122, no. 3, pp. 571–579, Mar. 2017.

[19] M. Schönke, M. Björnholm, A. V. Chibalin, J. R. Zierath, and A. S. Deshmukh, "Proteomics Analysis of Skeletal Muscle from Leptin-Deficient ob/ob Mice Reveals Adaptive Remodeling of Metabolic Characteristics and Fiber Type Composition," *Proteomics*, vol. 18, no. 5–6, p. 1700375, Mar. 2018.

[20] P. Zabielski *et al.*, "Altered skeletal muscle mitochondrial proteome as the basis of disruption of mitochondrial function in diabetic mice," *Diabetes*, vol. 65, no. 3, pp. 561–573, Mar. 2016.

[21] M. Kleinert *et al.*, "Quantitative proteomic characterization of cellular pathways associated with altered insulin sensitivity in skeletal muscle following high-fat diet feeding and

exercise training," *Sci. Rep.*, vol. 8, no. 1, pp. 1–11, Dec. 2018.

[22] F. Lang *et al.*, "Dynamic changes in the mouse skeletal muscle proteome during denervation-induced atrophy," *DMM Dis. Model. Mech.*, vol. 10, no. 7, pp. 881–896, Jul. 2017.

[23] L. Liu *et al.*, "Comparative label-free mass spectrometric analysis of temporal changes in the skeletal muscle proteome after impact trauma in rats," *Am. J. Physiol. Metab.*, p. ajpendo.00433.2019, Apr. 2020.

[24] C. Barbe *et al.*, "Comparative Proteomic and Transcriptomic Analysis of Follistatin-Induced Skeletal Muscle Hypertrophy," 2017.

[25] A. S. Barrett *et al.*, "Hydroxylamine Chemical Digestion for Insoluble Extracellular Matrix Characterization," 2017.

[26] K. Jacobson, A. Acuna, Y. Bu, Y. Leng, and S. Calve, "Distribution of the Extracellular Matrix Proteome Across the Myotendinous Junction," *J Proteome Res.* Under review.

[27] D. C. Dieterich, A. J. Link, J. Graumann, D. A. Tirrell, and E. M. Schuman, "Selective identification of newly synthesized proteins in mammalian cells using bioorthogonal noncanonical amino acid tagging (BONCAT)," *Proc. Natl. Acad. Sci. U. S. A.*, vol. 103, no. 25, pp. 9482–9487, Jun. 2006.

[28] F. I. Hinz, D. C. Dieterich, D. A. Tirrell, and E. M. Schuman, "Noncanonical Amino Acid Labeling in Vivo to Visualize and Affinity Purify Newly Synthesized Proteins in Larval Zebrafish," 2011.

[29] V. V. Rostovtsev, L. G. Green, V. V. Fokin, and K. B. Sharpless, "A Stepwise Huisgen Cycloaddition Process: Copper(I)-Catalyzed Regioselective 'Ligation' of Azides and Terminal Alkynes," *Angew. Chemie Int. Ed.*, vol. 41, no. 14, pp. 2596–2599, Jul. 2002.

[30] S. Calve, A. J. Witten, A. R. Ocken, and T. L. Kinzer-Ursem, "Incorporation of non-canonical amino acids into the developing murine proteome," *Sci. Rep.*, vol. 6, no. August, pp. 1–7, 2016.

[31] A. M. Saleh, K. R. Jacobson, T. L. Kinzer-Ursem, and S. Calve, "Dynamics of Non-Canonical Amino Acid-Labeled Intra- and Extracellular Proteins in the Developing Mouse," *Cell. Mol. Bioeng.*, vol. 12, no. 5, pp. 495–509, Oct. 2019.

[32] J. Cox and M. Mann, "MaxQuant enables high peptide identification rates, individualized p.p.b.-range mass accuracies and proteome-wide protein quantification," *Nat. Biotechnol.*,

vol. 26, no. 12, pp. 1367–1372, Dec. 2008.

[33] A. Naba, K. R. Clauser, H. Ding, C. A. Whittaker, S. A. Carr, and R. O. Hynes, "The extracellular matrix: Tools and insights for the 'omics' era," *Matrix Biology*, vol. 49. Elsevier B.V., pp. 10–24, 01-Jan-2016.

[34] M. Ashburner *et al.*, "Gene ontology: Tool for the unification of biology," *Nature Genetics*, vol. 25, no. 1. pp. 25–29, May-2000.

[35] S. A. Jelinsky, J. Archambault, L. Li, and H. Seeherman, "Tendon-selective genes identified from rat and human musculoskeletal tissues," *J. Orthop. Res.*, vol. 28, no. 3, p. n/a-n/a, Mar. 2009.

[36] K. Gelse, E. Pöschl, and T. Aigner, "Collagens - Structure, function, and biosynthesis," *Adv. Drug Deliv. Rev.*, vol. 55, no. 12, pp. 1531–1546, Nov. 2003.

[37] A. R. Gillies and R. L. Lieber, "Structure and function of the skeletal muscle extracellular matrix," *Muscle Nerve*, vol. 44, no. 3, p. n/a-n/a, Sep. 2011.

[38] R. Timpl and J. C. Brown, "Supramolecular assembly of basement membranes," *BioEssays*, vol. 18, no. 2, pp. 123–132, Feb. 1996.

[39] J. R. Sanes, "The basement membrane/basal lamina of skeletal muscle," *Journal of Biological Chemistry*, vol. 278, no. 15. American Society for Biochemistry and Molecular Biology, pp. 12601–12604, 11-Apr-2003.

[40] S. S. Rayagiri *et al.*, "Basal lamina remodeling at the skeletal muscle stem cell niche mediates stem cell self-renewal," *Nat. Commun.*, vol. 9, no. 1, pp. 1–12, Dec. 2018.

[41] J. H. Miner, G. Go, J. Cunningham, B. L. Patton, and G. Jarad, "Transgenic isolation of skeletal muscle and kidney defects in laminin β2 mutant mice: Implications for Pierson syndrome," *Development*, vol. 133, no. 5, pp. 967–975, Mar. 2006.

[42] F. Bost, M. Diarra-Mehrpour, and J.-P. Martin, "Inter-alpha-trypsin inhibitor proteoglycan family. A group of proteins binding and stabilizing the extracellular matrix," *Eur. J. Biochem.*, vol. 252, no. 3, pp. 339–346, Mar. 1998.

[43] D. Nikitovic, J. Aggelidakis, M. F. Young, R. V. Iozzo, N. K. Karamanos, and G. N. Tzanakakis, "The biology of small leucine-rich proteoglycans in bone pathophysiology," *J. Biol. Chem.*, vol. 287, no. 41, pp. 33926–33933, Oct. 2012.

[44] M. Hara *et al.*, "Periostin Promotes Fibroblast Migration and Inhibits Muscle Repair After Skeletal Muscle Injury," *J. Bone Jt. Surg.*, vol. 100, no. 16, p. e108, Aug. 2018.

[45] S. M. L. Terena, K. P. S. Fernandes, S. K. Bussadori, A. M. Deana, and R. A. Mesquita-Ferrari, “Systematic review of the synergist muscle ablation model for compensatory hypertrophy,” *Revista da Associacao Medica Brasileira*, vol. 63, no. 2. Associacao Medica Brasileira, pp. 164–172, 01-Feb-2017.

[46] M. Lehto, T. J. Sims, and A. J. Bailey, “Skeletal Muscle Injury Molecular Changes in the Collagen During Healing*,” 1985.

[47] R. Csapo, M. Gumpenberger, and B. Wessner, “Skeletal Muscle Extracellular Matrix – What Do We Know About Its Composition, Regulation, and Physiological Roles? A Narrative Review,” *Front. Physiol.*, vol. 11, p. 253, Mar. 2020.

PUBLICATIONS

A. F. Miller, “Identifying Extracellular Matrix Protein Turnover Rates for Tissue Engineers,” *J. Purdue Undergrad. Res.*, vol. 9, no. 1, Aug. 2019.

In preparation: T. C. Davis, A. F. Miller, S. Calve, S. A. Claridge, “2D Scaffold for Directing Cell Growth.”